Supporting Information

for publication

Exploring the solid form landscape of antifungal drug Isavuconazole: crystal structure analysis, phase transformation behavior and dissolution performance

*Alexander P. Voronin[a], Nikita A. Vasilev[a], Artem O. Surov[a], Andrei V. Churakov[b], German L. Perlovich[a]**

[a]G.A. Krestov Institute of Solution Chemistry of the Russian Academy of Sciences, 1 Akademicheskaya St., 153045 Ivanovo, Russia

[b]N.S. Kurnakov Institute of General and Inorganic Chemistry RAS, 31 Leninsky Prosp., 119991, Moscow, Russia.

*To whom correspondence should be addressed: Telephone: +7-4932-533784; Fax: +7-4932- 336237; E-mail glp@isc-ras.ru

Table S1. Results of the polymorph/solvate screening of ISV using different experimental techniques

Method	Solvent	Results
Solution crystallization	Acetone	ISV
Solution crystallization	Methanol	ISV
Solution crystallization	Ethanol	ISV
Solution crystallization	2-propanol	ISV
Solution crystallization	Acetonitrile	ISV
Solution crystallization	Dimethylsulfoxide	ISV
Solution crystallization	N,N-Dimethylformamide	ISV
Solution crystallization	Acetonitrile-H_2O (1:1)	[ISV+H_2O] (1:1)
Solution crystallization	2-propanol-H_2O (3:1)	[ISV+H_2O] (1:1)
Solution crystallization	Chlorophorm-methanol (1:2)	ISV
Solution crystallization	$CHCl_3$	noncrystalline
Solution crystallization	Dioxane	noncrystalline
Solution crystallization	Tetrahydrofuran	noncrystalline
Freeze drying	tert-Butyl alcohol-H_2O (33:67)	Amorphous
Freeze drying	tert-Butyl alcohol-H_2O (50:50)	Amorphous
Freeze drying	tert-Butyl alcohol-H_2O (60:40)	Amorphous
Freeze drying	tert-Butyl alcohol-H_2O (67:33)	Amorphous
Freeze drying	tert-Butyl alcohol	Amorphous
Neat grinding	-	Amorphous

Table S2. Results of mechanochemical screening of isavuconazole (ISV) with organic acids of different classes

Salt former	Molecular structure	Molar ratio (ISV:Coformer)	Solvent	Results
Dicarboxylic acids				
Glycolic acid	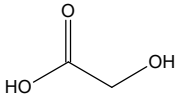	1:1	H_2O	ISV
			ACN	noncrystalline
Malonic acid	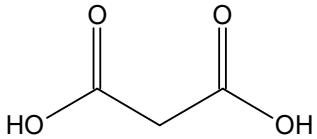	1:1	H_2O	[ISV-H_2O] + CF
			ACN	noncrystalline
		2:1	H_2O	[ISV-H_2O] + CF
			ACN	noncrystalline
		1:2	H_2O	[ISV-H_2O] + CF
			ACN	noncrystalline
Maleic acid	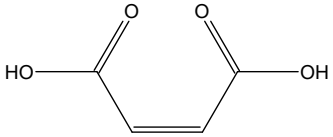	1:1	H_2O	noncrystalline
			ACN	noncrystalline
		2:1	H_2O	noncrystalline
			ACN	noncrystalline
		1:2	H_2O	noncrystalline
			ACN	noncrystalline
Fumaric acid	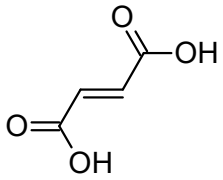	1:1	H_2O	[ISV-H_2O] + CF
			ACN	noncrystalline
		2:1	H_2O	[ISV-H_2O] + CF
			ACN	noncrystalline
		1:2	H_2O	[ISV-H_2O] + CF
			ACN	noncrystalline
Succinic acid	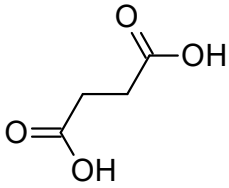	1:1	H_2O	ISV + [ISV-H_2O]
			ACN	noncrystalline
		2:1	H_2O	[ISV-H_2O]
			ACN	noncrystalline
		1:2	H_2O	[ISV-H_2O] + CF
			ACN	noncrystalline

Malic acid	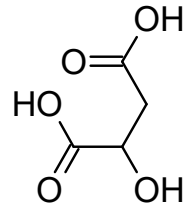	1:1	H_2O	ISV + [ISV-H_2O] + CF
			ACN	noncrystalline
		2:1	H_2O	[ISV-H_2O]
			ACN	noncrystalline
		1:2	H_2O	[ISV-H_2O] + CF
			ACN	noncrystalline
Tartaric acid	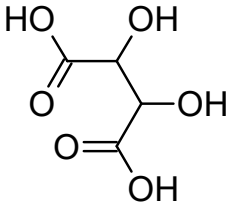	1:1	H_2O	ISV + [ISV-H_2O] + CF
			ACN	noncrystalline
		2:1	H_2O	[ISV-H_2O]
			ACN	noncrystalline
		1:2	H_2O	[ISV-H_2O] + CF
			ACN	noncrystalline
Glutaric acid	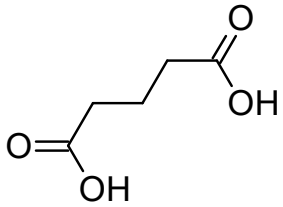	1:1	H_2O	[ISV-H_2O] + CF
			ACN	noncrystalline
		2:1	H_2O	[ISV-H_2O] + CF
			ACN	noncrystalline
		1:2	H_2O	[ISV-H_2O] + CF
			ACN	noncrystalline
trans-Aconitic acid	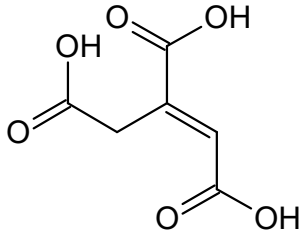	1:1	H_2O	[ISV-H_2O] + CF
			ACN	noncrystalline
		2:1	H_2O	[ISV-H_2O] + CF
			ACN	noncrystalline
		1:2	H_2O	[ISV-H_2O] + CF
			ACN	noncrystalline
Citric acid	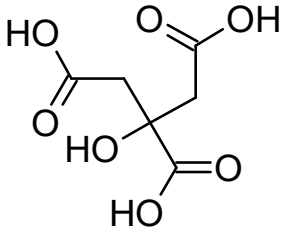	1:1	H_2O	noncrystalline
			ACN	noncrystalline
		2:1	H_2O	noncrystalline
			ACN	noncrystalline
		1:2	H_2O	noncrystalline
			ACN	noncrystalline

Adipic acid	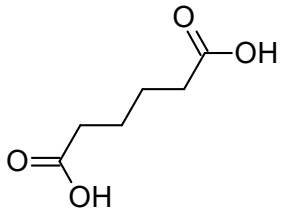	1:1	H_2O	ISV + [ISV-H_2O] + CF
			ACN	noncrystalline
		2:1	H_2O	ISV + [ISV-H_2O]
			ACN	noncrystalline
		1:2	H_2O	[ISV-H_2O] + CF
			ACN	noncrystalline
Pimelic acid	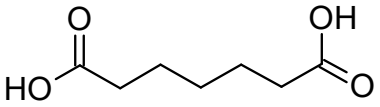	1:1	H_2O	[ISV-H_2O]+ CF
			ACN	noncrystalline
		2:1	H_2O	[ISV-H_2O]+ CF
			ACN	noncrystalline
		1:2	H_2O	[ISV-H_2O]+ CF
			ACN	noncrystalline
Aromatic acids				
Benzoic acid	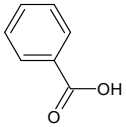	1:1	H_2O	[ISV-H_2O] + CF
			ACN	noncrystalline
Salicylic acid	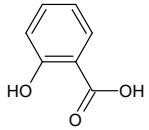	1:1	H_2O	ISV + CF
			ACN	noncrystalline
4-Hydroxybenzoic acid	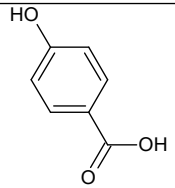	1:1	H_2O	[ISV-H_2O]+ ISV + CF
			ACN	noncrystalline
Gallic acid	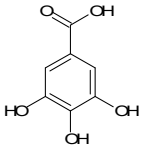	1:1	H_2O	[ISV-H_2O] + CF
			ACN	noncrystalline

Vanillic acid	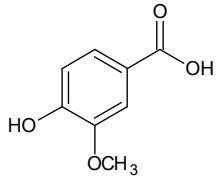	1:1	H_2O	[ISV-H_2O]
			ACN	noncrystalline
4-Aminobenzoic acid	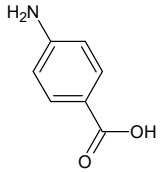	1:1	H_2O	[ISV-H_2O] + CF
			ACN	noncrystalline
Terephthalic acid	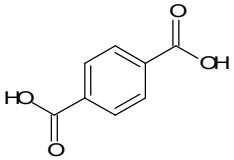	1:1	H_2O	[ISV-H_2O] + ISV + CF
			ACN	noncrystalline
Sulfonic acids				
Saccharine	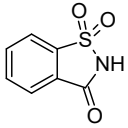	1:1	H_2O	[ISV-H_2O]+ CF
			ACN	noncrystalline
Acesulfame	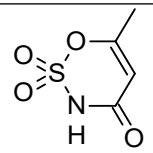	1:1	H_2O	ISV + CF
			ACN	noncrystalline
Methanesulfonic acid	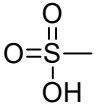	1:10	H_2O	ISV + [ISV-H_2O] + CF
		1:10	ACN	noncrystalline
p-Toluenesulfonic acid	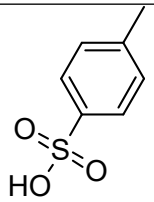	1:1	H_2O	noncrystalline
			ACN	[ISV-TS-ACN]

Table S3. Results of slurry screening of isavuconazole (ISV) with inorganic acids

Inorganic acids				
Salt former	Molecular structure	Molar ratio (ISV:Coformer)	Solvent	Results
Orthophosphoric acid	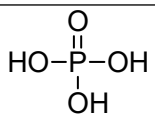	1:10	EtOH-H_2O (1:1)	[ISV-P] (1:1)
Sulfuric acid	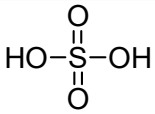	1:10	H_2O	[ISV-H_2O] (1:1)
Hydrochloric acid	HCl	1:10	MeOH-H_2O (1:1)	[ISV-H_2O] (1:1)

Table S4. Crystallographic data for obtained crystal forms of ISV

	ISV	[**ISV-H_2O**] (1:1)	[**ISV-TS-ACN**] (1:1:0.212)	[**ISV-P**] (1:1)
Crystal data				
CCDC no.	2113413	2113411	2113410	2113412
Chemical formula	$C_{22}H_{17}F_2N_5OS$	$C_{22}H_{17}F_2N_5OS\cdot H_2O$	$C_{22}H_{18}F_2N_5OS\cdot C_7H_7O_3S\cdot 0.212(C_2H_3N)$	$C_{22}H_{17.52}F_2N_5OS\cdot H_{2.48}O_4P$
M_r	437.46	455.48	618.35	535.46
Crystal system	Monoclinic	Orthorhombic	Monoclinic	Orthorhombic
Space group	$P2_1$	$P2_12_12_1$	$C2$	$P2_12_12_1$
Temperature (K)	100	150	150	100
a (Å)	5.8250 (3)	7.8920 (2)	29.078 (4)	6.1215 (3)
b (Å)	17.3293 (8)	11.2256 (3)	8.7230 (12)	11.1722 (5)
c (Å)	9.7547 (4)	24.2967 (6)	12.0174 (16)	34.3989 (17)
α (°)	90	90	90	90
β (°)	97.072 (2)	90	93.915 (6)	90
γ (°)	90	90	90	90
V (Å^3)	977.18 (8)	2152.50 (10)	3041.1 (7)	2352.56 (19)
Z	2	4	4	4
Radiation type	Mo $K\alpha$	Mo $K\alpha$	Mo $K\alpha$	Mo $K\alpha$
μ (mm^{-1})	0.21	0.20	0.23	0.27
Crystal size (mm)	0.25×0.20×0.10	0.30×0.12×0.10	0.40×0.12×0.03	0.30×0.10×0.05
Data collection				
T_{min}, T_{max}	0.394, 0.754	0.664, 0.746	0.356, 0.752	0.402, 0.753
Reflns. measured	42105	18824	8833	26066
Independent reflns.	5667	4693	5000	6870
observed reflns. with [$I > 2s(I)$]	5522	4447	4268	6622
R_{int}	0.032	0.024	0.042	0.030
$(\sin q/l)_{max}$ (Å^{-1})	0.703	0.639	0.617	0.703
Refinement				
$R[F^2 > 2s(F^2)]$, $wR(F^2)$, S	0.026, 0.066, 1.05	0.029, 0.071, 1.03	0.062, 0.145, 1.05	0.028, 0.067, 1.06
No. of reflections	5667	4693	5000	6870
No. of parameters	348	365	416	408
No. of restraints	1	0	13	0
$(\Delta/\sigma)_{max}$	< 0.001	0.001	< 0.001	0.002
$\Delta\rangle_{max}$, $\Delta\rangle_{min}$ (e Å^{-3})	0.31, -0.19	0.20, -0.16	0.31, -0.34	0.30, -0.28

Table S5. Contributions into the crystal lattice energy from the components and different kinds of non-covalent interactions in the crystal forms of ISV estimated by QTAIMC and given in $kJ \cdot mol^{-1}$ and % of total lattice energy value.

Crystal	ISV_{CR}	[ISV-H_2O] (1:1)	[ISV-TS] (1:1)	[ISV-TS-ACN] (1:1:1)	[ISV-P] (1:1) salt	[ISV-P] (1:1) cocrystal
E_{latt}(0K)	**136.4**	**214.5**	**237.4**	**305.1**	**366.6**	**337.5**
ΣE_{int}(H-bonds)	0 (0%)	93.9 (43.8%)	39.5 (16.6%)	40.6 (13.3%)	186.7 (50.9%)	165.1 (48.9%)
ΣE_{int}(C-H···X)	55.5 (39.3%)	87.3 (40.7%)	120.2 (50.6%)	160.8(52.7%)	106.6 (29.1%)	103.7(30.7%)
ΣE_{int}(C-H···π)	16.4 (11.6%)	18.2 (8.5%)	28.6 (12.0%)	37.8 (12.4%)	5.949 (1.6%)	6.5 (1.9%)
ΣE_{int}(π···π)	58.3 (41.3%)	6.3 (2.9%)	40.6 (17.1%)	50.4 (16.5%)	62.7 (17.1%)	62.3 (18.5%)
ΣE_{int}(vdW)	11.2 (7.9%)	8.8 (4.1%)	8.6 (3.6%)	15.5 (5.1%)	4.6 (1.3%)	2.3 (0.7%)
ΣE_{int}(ISV–ISV)	–	89.8 (41.9%)	62.6 (26.4%)	65.6 (21.5%)	99.3 (27.1%)	106.0 (31.4%)
ΣE_{int}(ISV–CF)	–	124.7 (58.1%)	173.6 (73.1%)	173.8 (57.0%)	157.1 (42.9%)	123.7 (36.6%)
ΣE_{int}(CF–CF)	–	0 (0%)	1.1 (0.5%)	0 (0%)	110.1 (30.0%)	107.8 (32.0%)
ΣE_{int}(ISV–ACN)	–	–	–	49.1 (16.1%)	–	–
ΣE_{int}(CF–ACN)	–	–	–	13.7 (4.5%)	–	–
ΣE_{int}(ACN–ACN)	–	–	–	2.9 (0.9%)	–	–
ΣE_{int}(ISV)	–	152.1 (70.9%)	149.4 (63.0%)	177.1 (58.0%)	177.9 (48.5%)	167.8 (49.7%)
ΣE_{int}(CF)	–	62.3 (29.1%)	88.0 (37.0%)	93.7 (30.7%)	188.7 (51.5%)	169.7 (50.3%)
ΣE_{int}(ACN)	–	–	–	34.3 (11.2%)	–	–

CF = coformer

X = C, O, N, F

S1. Evaluation of performance of different theoretical schemes for lattice energy evaluation

In order to study in details the energetics of crystal forms of an API, one needs to ensure that the applied method provides reliable and accurate results. The best criterion for a valid theoretical method is its capability to reproduce the experimental data. Most commonly used approaches for lattice energy estimation are usually validated against a benchmark set of simple organic molecules that may be irrelevant to "real-life" pharmaceuticals. As it was demonstrated by our group, see Refs. [1, 2], well-proven methods can fail to reproduce the crystal lattice energy of some APIs. Therefore, testing multiple independent computational methods is required in order to avoid incorrect estimation of energetic features of solid forms.

In the present work, the crystal lattice energy of pure ISV was estimated using several computational methods based on different approaches: DFT-D3 (eq. 1), QTAIMC (eq. 3), and semi-empirical PIXEL, AA-CLP and CE-B3LYP schemes. The lattice energy at 298K was derived using a 2RT correction and compared with the recently determined experimental sublimation enthalpy value obtained by transpiration (138.1±0.5 kJ mol^{-1}). [3]

The values of theoretical lattice energies and sublimation enthalpy of pure ISV taken from the literature are summarized in Table S6. One can see that the E_{latt}(298K) value obtained from QTAIMC calculations (136.4 kJ mol^{-1}) is in a good agreement with the experiment, while other methods overestimate this value by 24-70%. Therefore, QTAIMC was used further as most appropriate method to describe lattice energies and energies of individual non-covalent interactions in multicomponent crystal forms of ISV.

Table S6. Comparison of theoretical and experimental lattice energies of pure ISV at 298 K obtained by different theoretical and experimental approaches

Calculated					Exp. [3]
DFT-D3	QTAIMC	PIXEL	AA-CLP	CE-B3LYP	
171.1	136.4	183.7	235.4	199.7	138.1±0.5

S2. Conformational stability of ISV molecules in different crystal forms.

In order to rationalize the fact that ISV_{CR} does not transfer into [ISV-H_2O] (1:1) when placed into contact with water we estimated the relative energies and the conformation barrier height of the isolated ISV molecules and ISV-H_2O complexes using the PCM model. The energetic barrier height between the "open" and "close" conformations in the solution equals to 25.1 kJ mol^{-1}, which exceeds the energy of thermal vibrations but is lower than the typical activation energy of the nucleation process.[4] (Scheme S1)

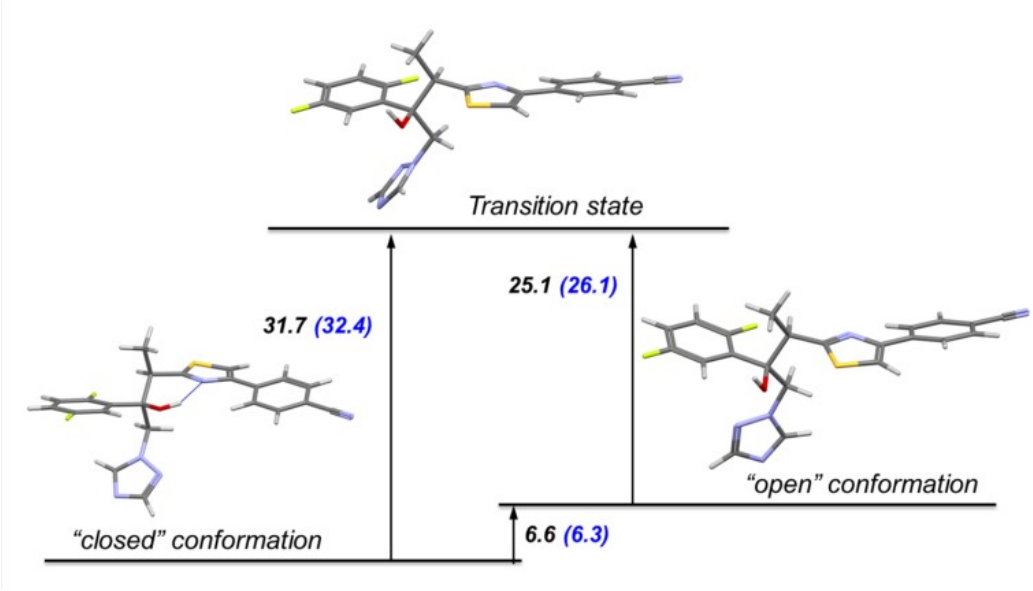

Scheme S1. Energy ranking of relaxed ISV molecules corresponding to "open" and "closed" conformations observed in ISV and [ISV-H_2O] crystal structures. The numbers indicate the relative energies between the conformations and the transition state of isolated ISV molecules (blue for ISV-H_2O complexes) in kJ mol^{-1}.

When a molecule of water is placed near the hydroxyl group, the relative energies do not change significantly, resulting in ΔE = 6.3 kJ·mol^{-1} and barrier height of 26.1 kJ·mol^{-1} (Figure 8). While the transition between the "open" and "closed" conformations is possible in solution, the size and shape of the ISV molecule make impossible the direct solid-solid transformation in the condensed state caused by the conformation change due to steric hindrances. This explains the absence of a crystalline phase after the thermal dehydration of [ISV-H_2O] (1:1) and kinetic stabilization of anhydrous ISV when the solid is placed in contact with water.

References:

1. A. N. Manin, A. P. Voronin, K. V. Drozd and G. L. Perlovich, *Thermochimica Acta*, 2019, **682**, 178411.
2. K. V. Drozd, A. N. Manin, A. P. Voronin and G. L. Perlovich, *The Journal of Chemical Thermodynamics*, 2021, **155**, 106369.
3. M. Ol'khovich, A. Sharapova, S. Blokhina and G. Perlovich, *Molecules*, 2021, **26**, 4759.
4. S. K. Tang, R. J. Davey, P. Sacchi and A. J. Cruz-Cabeza, *Chemical Science*, 2021, **12**, 993-1000.

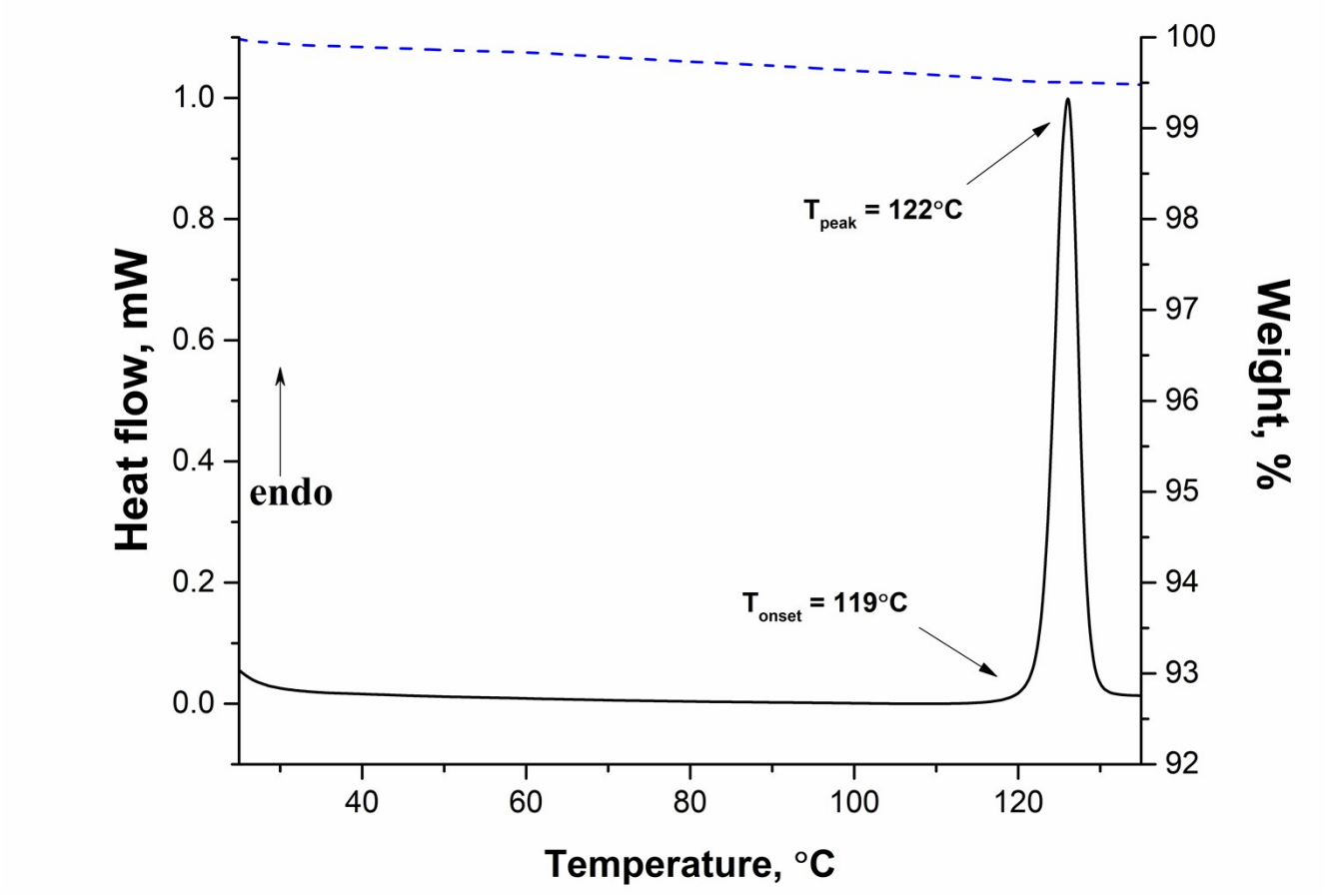

Figure S1. Results of DSC (solid line) and TG experiments (dashed line) for ISV_{CR}

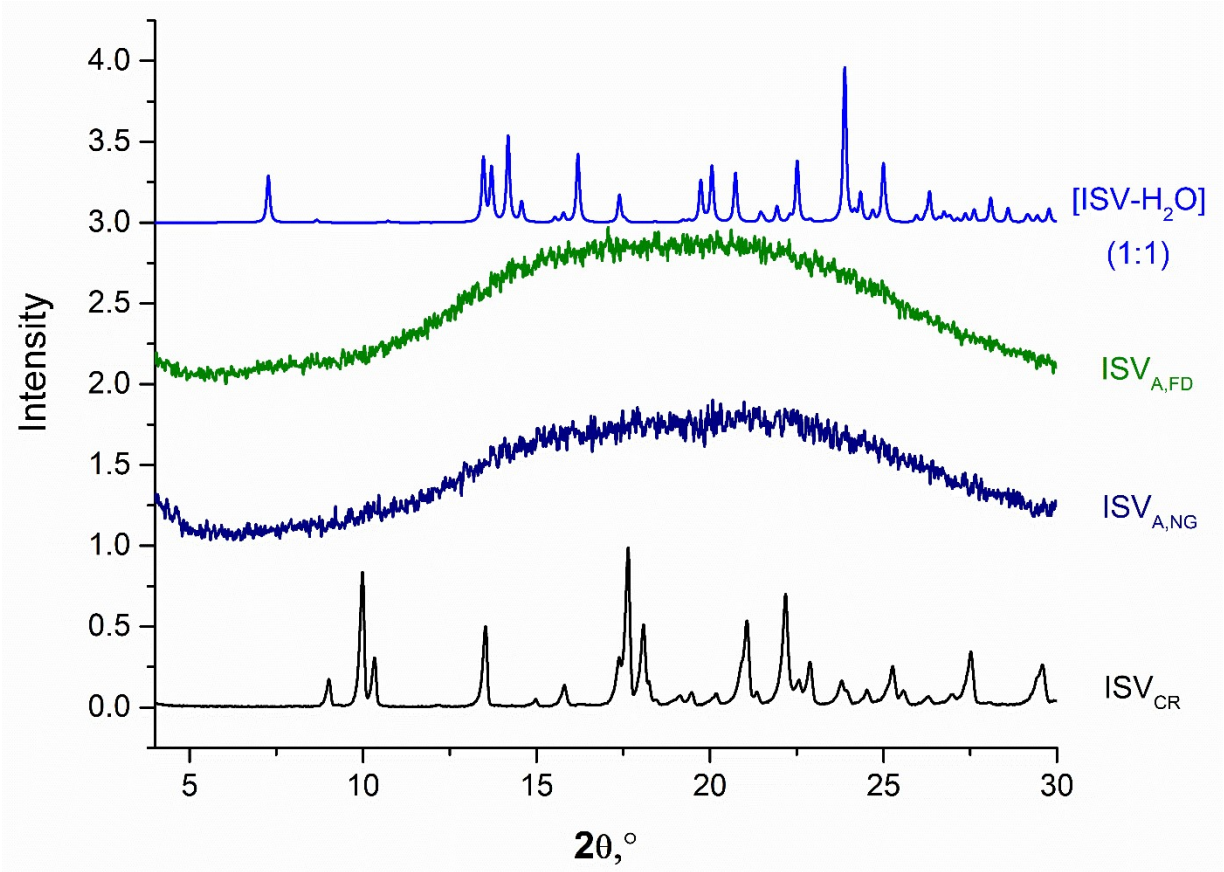

Figure S2. Experimental PXRD patterns of initial crystalline ISV (ISV_{CR}), ISV monohydrate ([ISV-H_2O]) and amorphous ISV obtained by neat grinding ($ISV_{A,NG}$) and freeze-drying ($ISV_{A,FD}$)

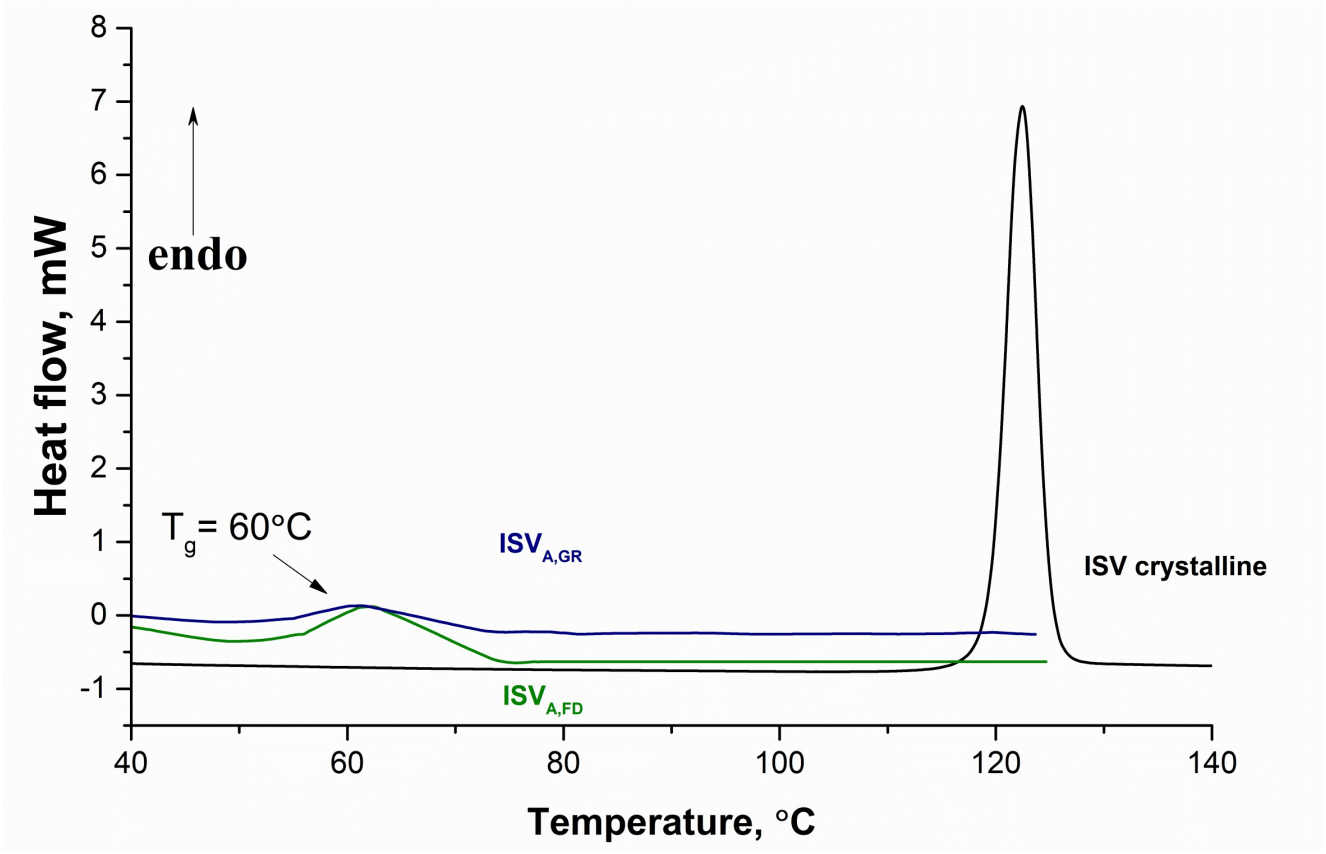

Figure S3. Overlay of DSC profiles of crystalline ISV and amorphous ISV obtained by neat grinding ($ISV_{A,NG}$) and freeze-drying ($ISV_{A,FD}$)

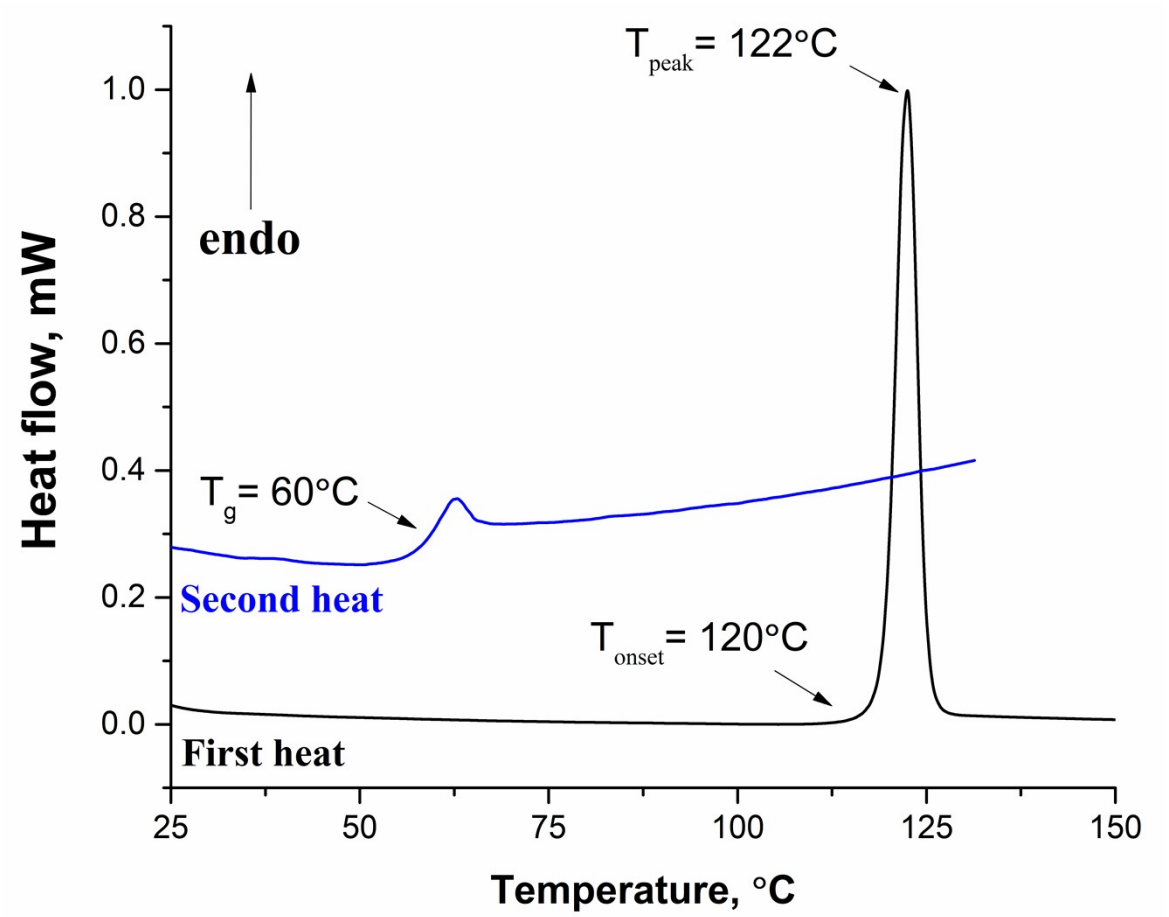

Figure S4. DSC profiles of crystalline ISV recorded during the cyclic heating experiment: initial sample (black line), sample after heating to 150 °C

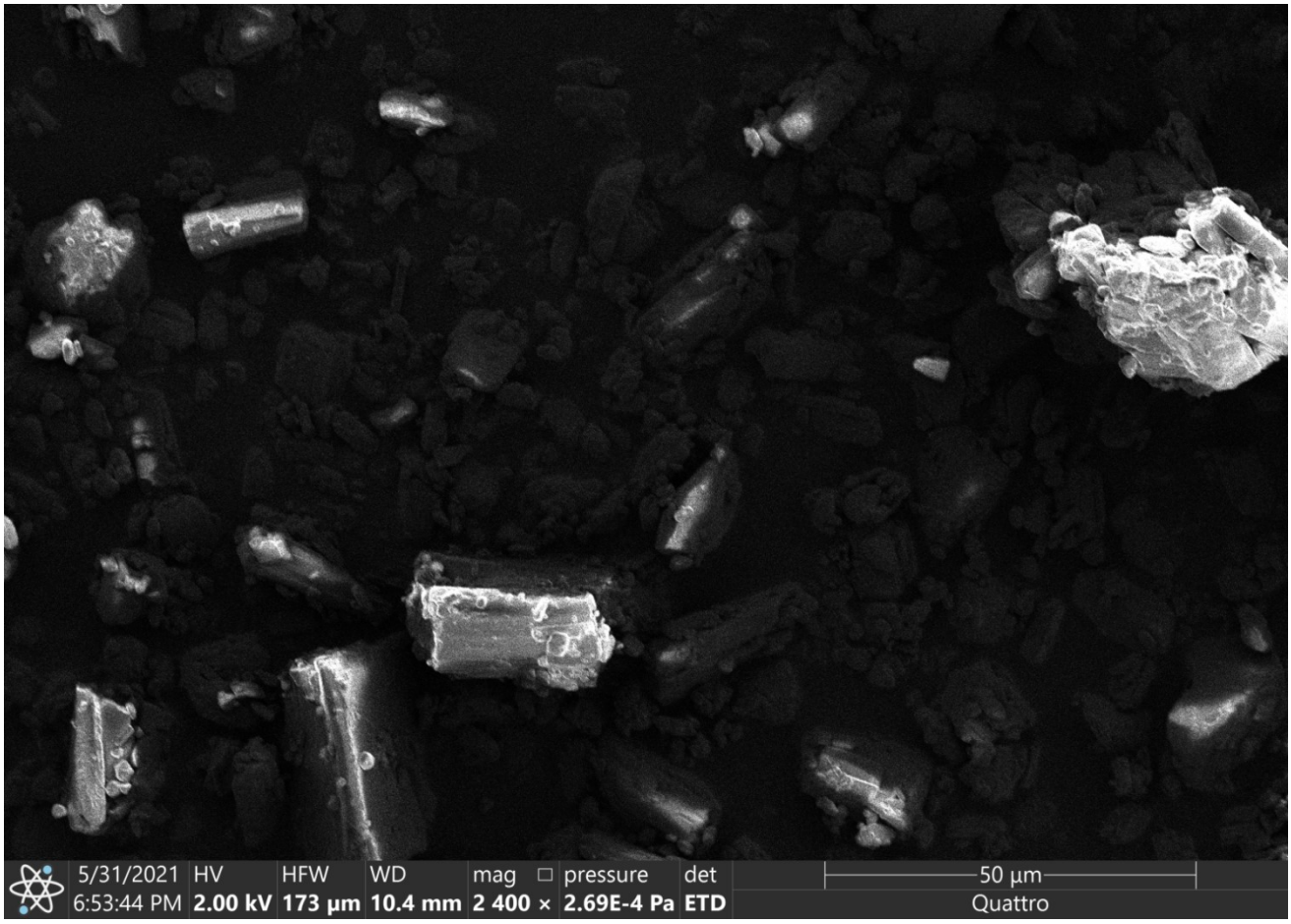
5/31/2021 HV HFW WD mag pressure det
6:53:44 PM 2.00 kV 173 µm 10.4 mm 2 400 × 2.69E-4 Pa ETD
50 µm
Quattro

(a)

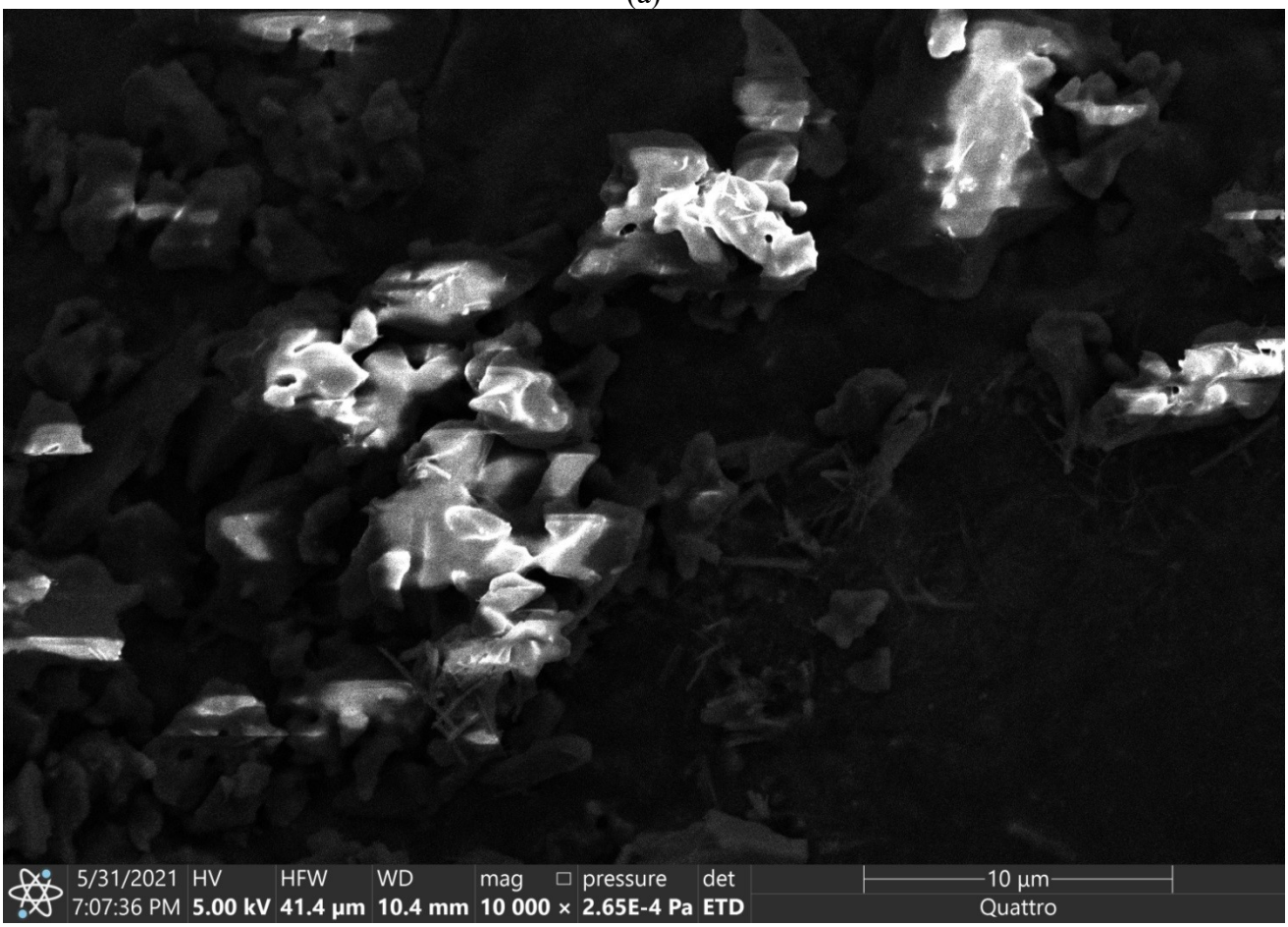
5/31/2021 HV HFW WD mag pressure det
7:07:36 PM 5.00 kV 41.4 µm 10.4 mm 10 000 × 2.65E-4 Pa ETD
10 µm
Quattro

(b)

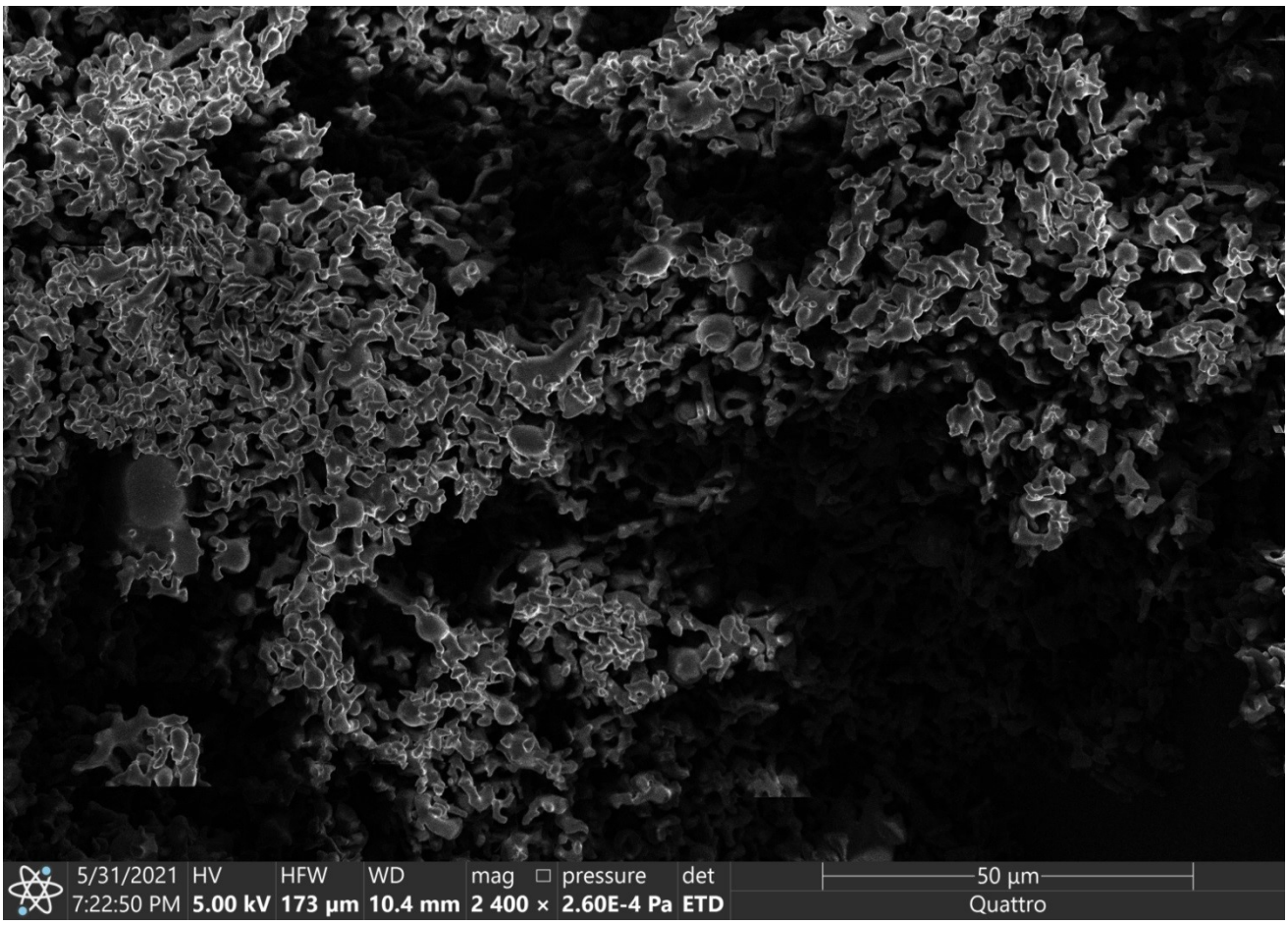

(c)

Figure S5. SEM images of initial ISV_{CR} (a), amorphous ISV obtained by neat grinding ($ISV_{A,NG}$) (b) and amorphous ISV obtained by freeze-drying ($ISV_{A,FD}$) (c)

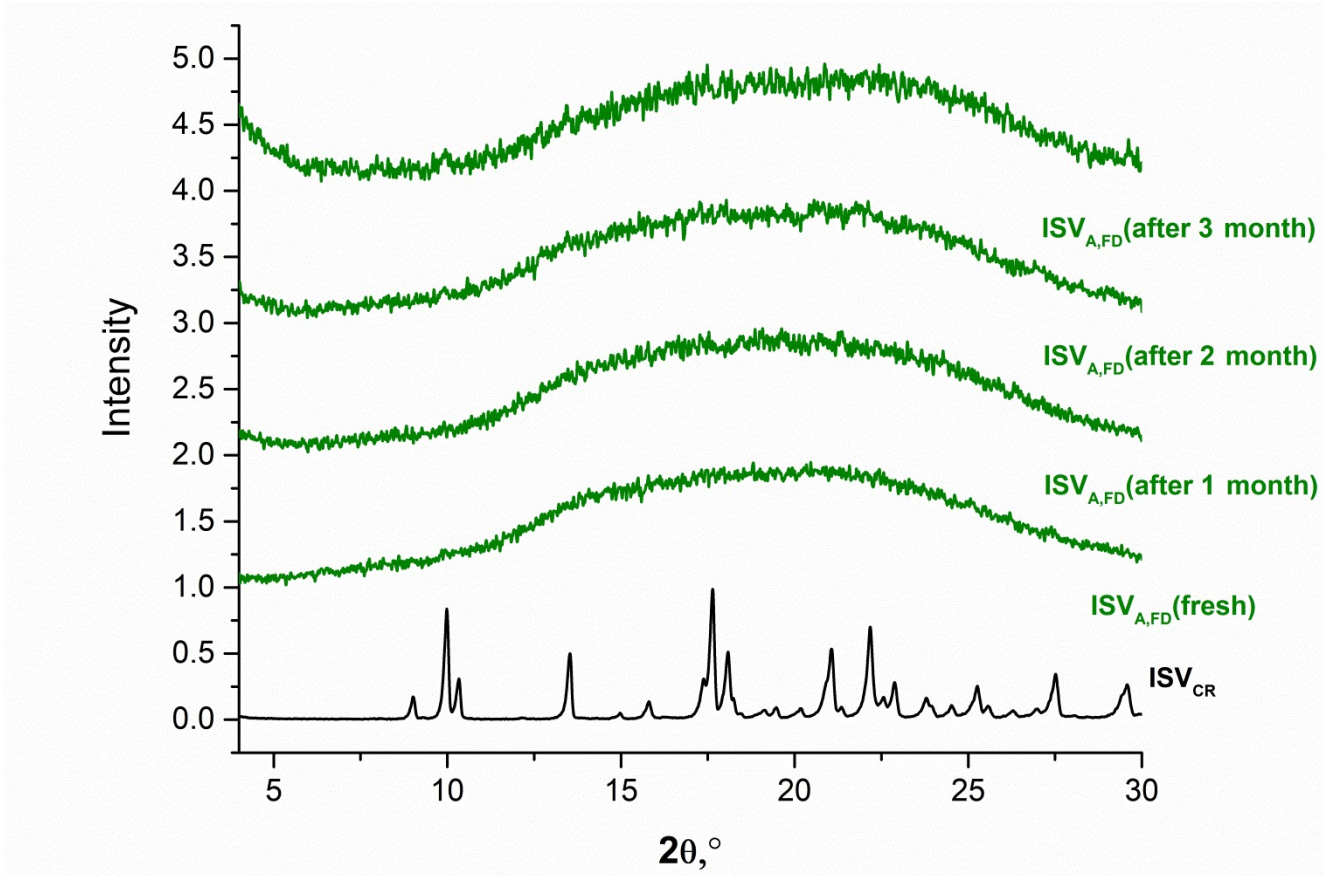

(a)

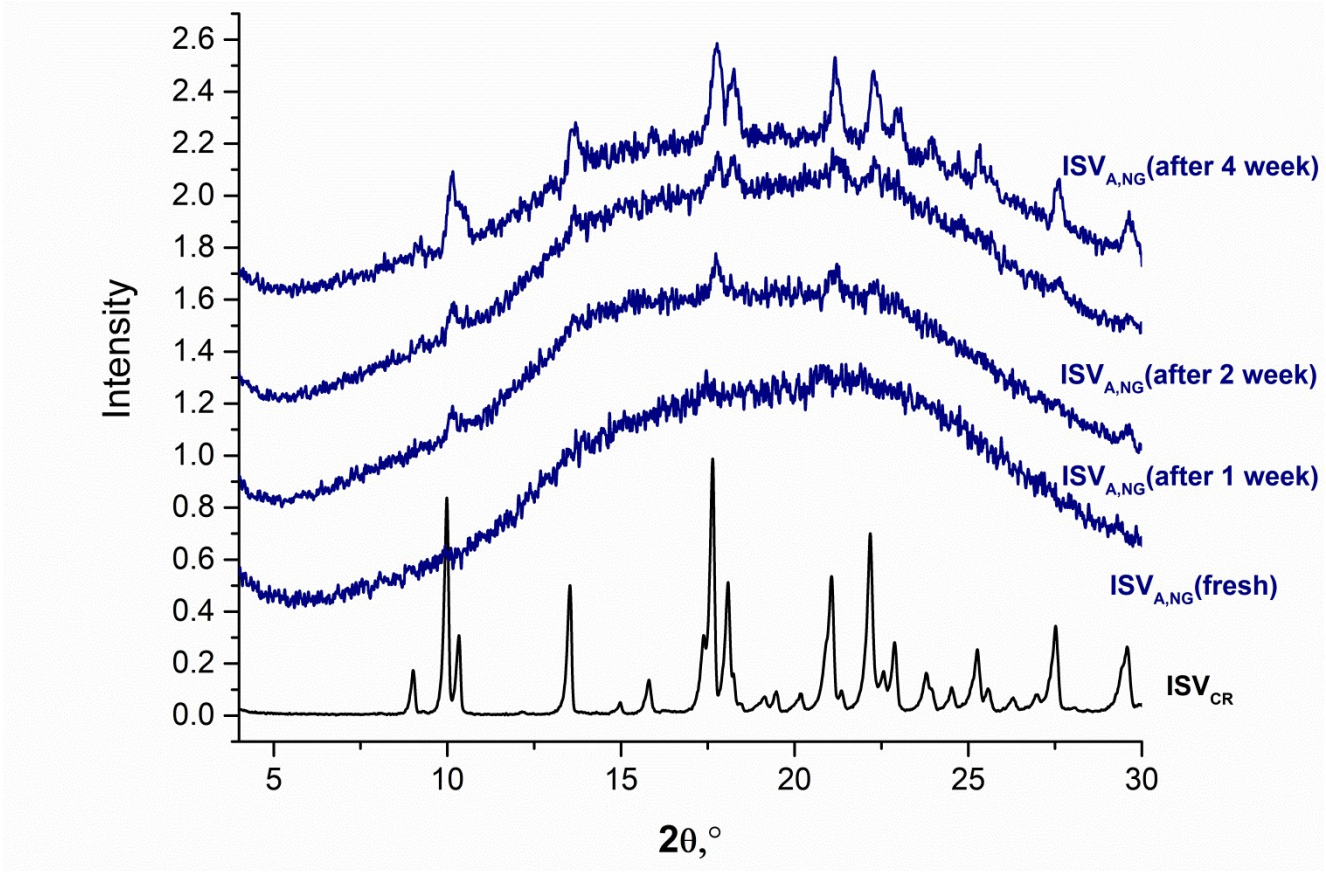

(b)

Figure S6. PXRD patterns of $ISV_{A,FD}$ (A) and $ISV_{A,NG}$ (B) after storage for different times at 0% RH at room temperature.

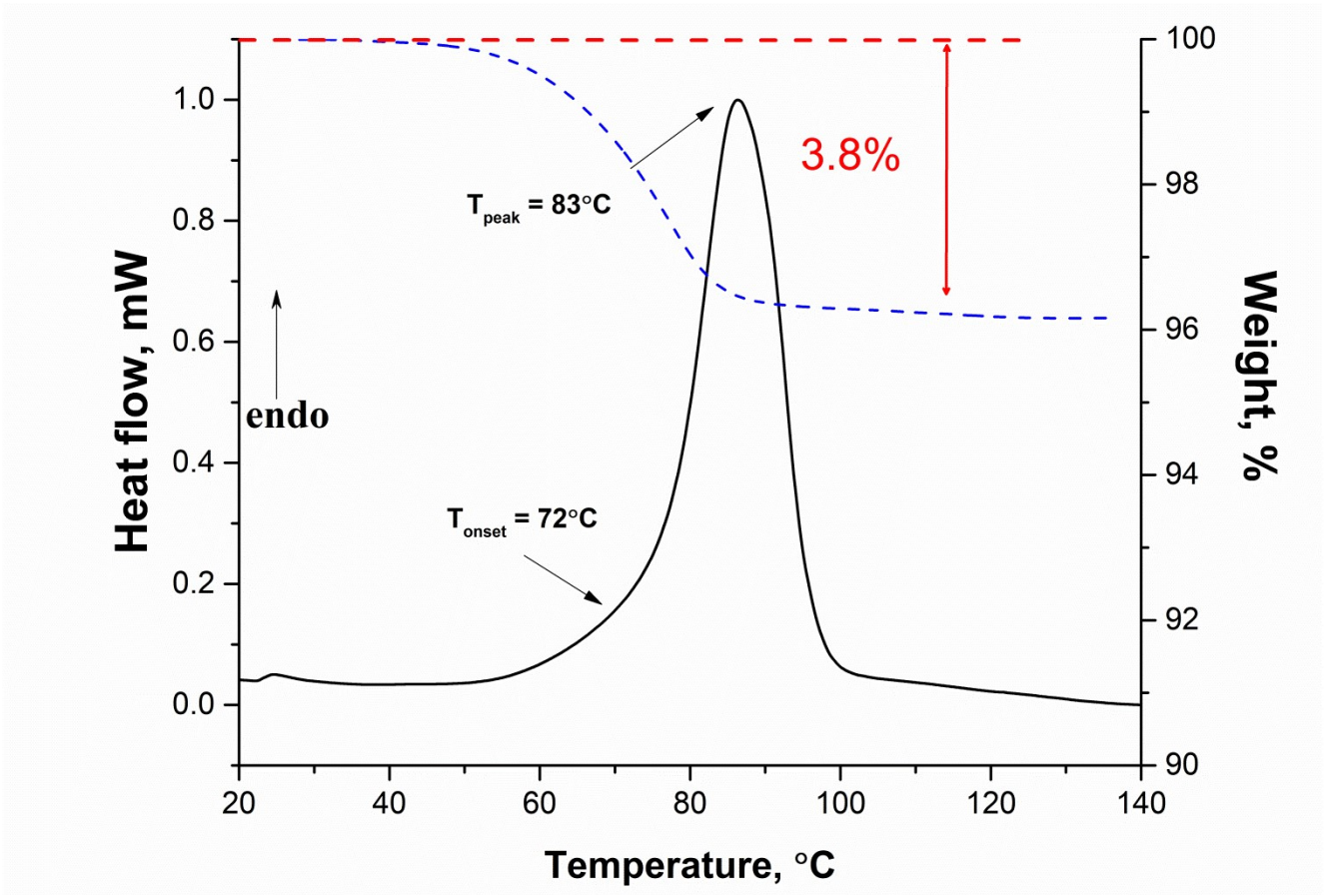

Figure S7. The results of DSC (solid line) and TG (dashed line) experiments for [ISV-H_2O].

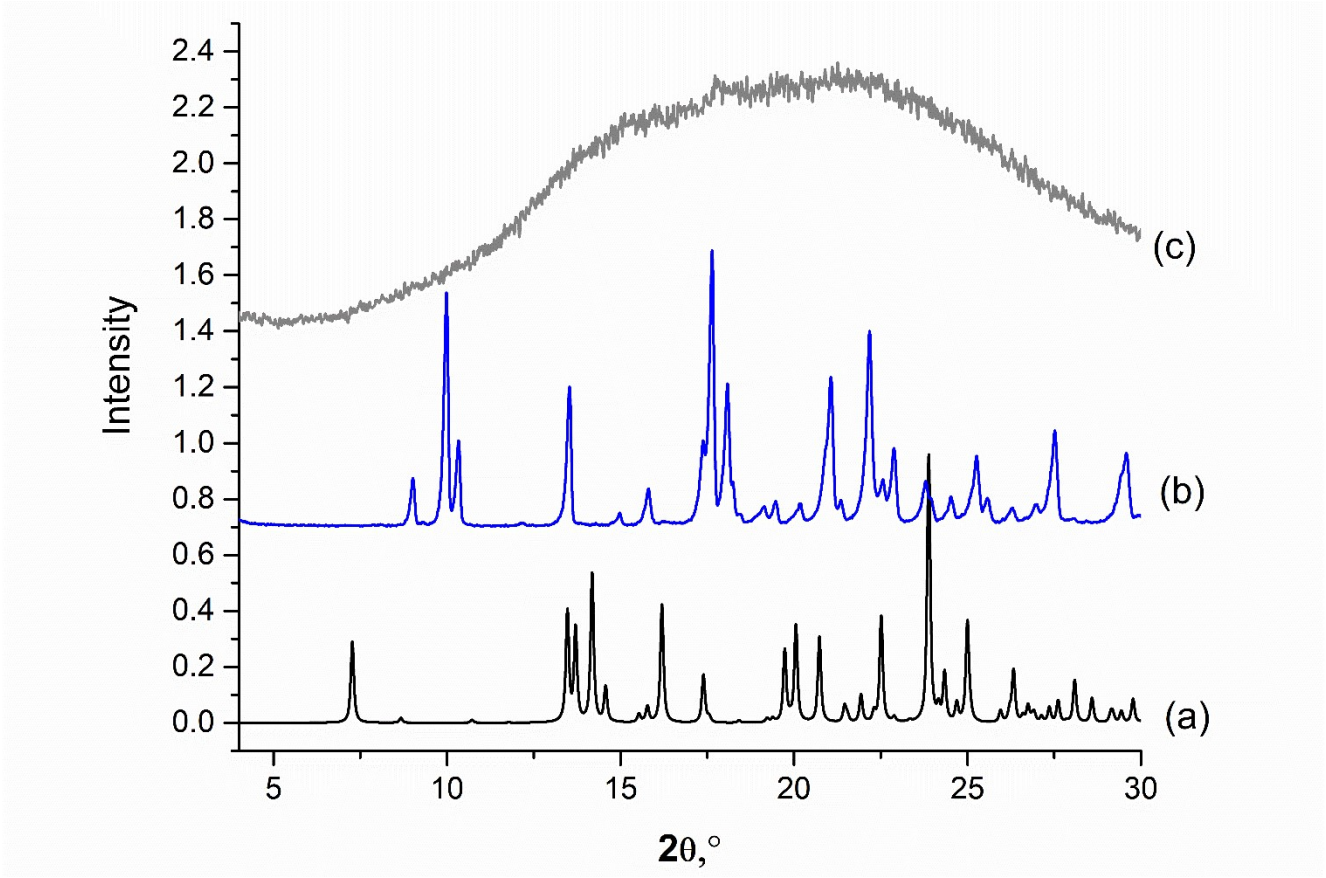

Figure S8. Powder XRD patterns of initial ISV (a), [ISV-H_2O] (b), and [ISV-H_2O] after heating above the dehydration temperature (c)

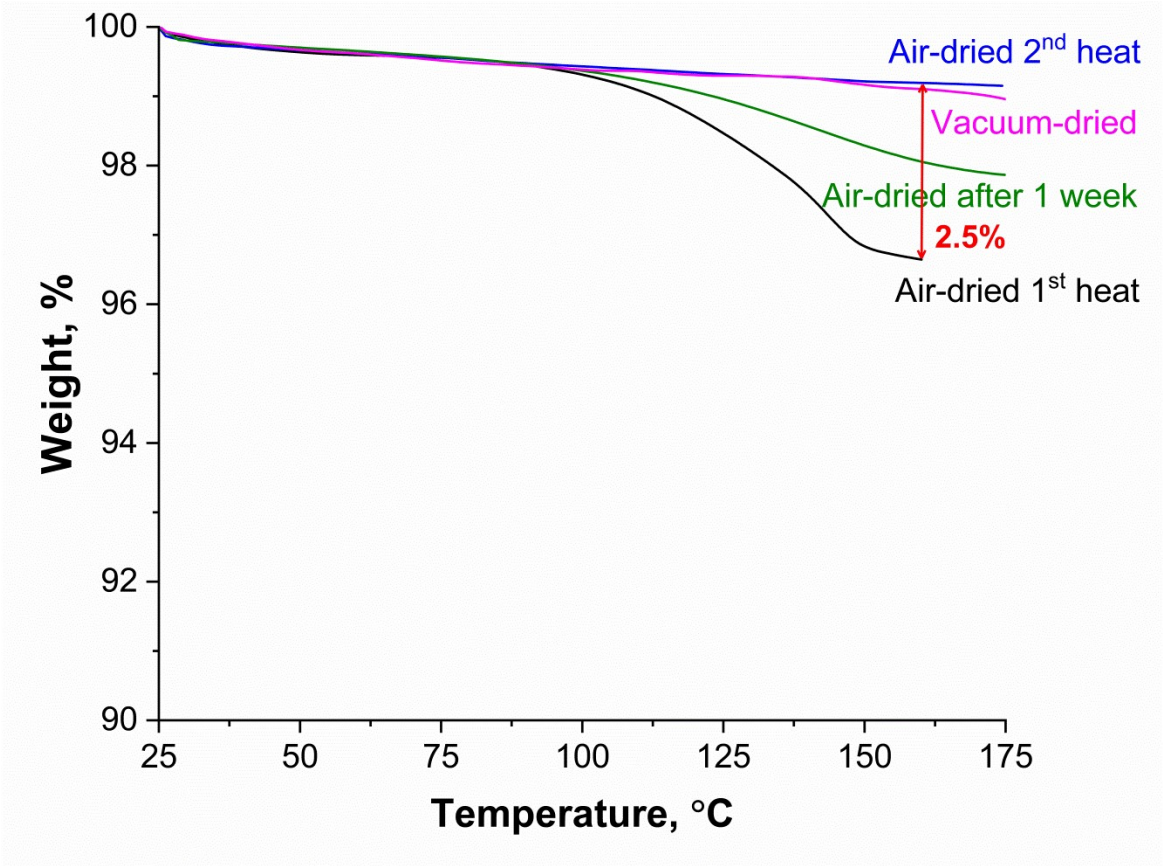

Figure S9. TG results for [ISV-TS-ACN] sample: initial sample (black line), after heating to 160 °C (blue line), stored for a week (green line); the sample dried under reduced pressure to constant mass (magenta line).

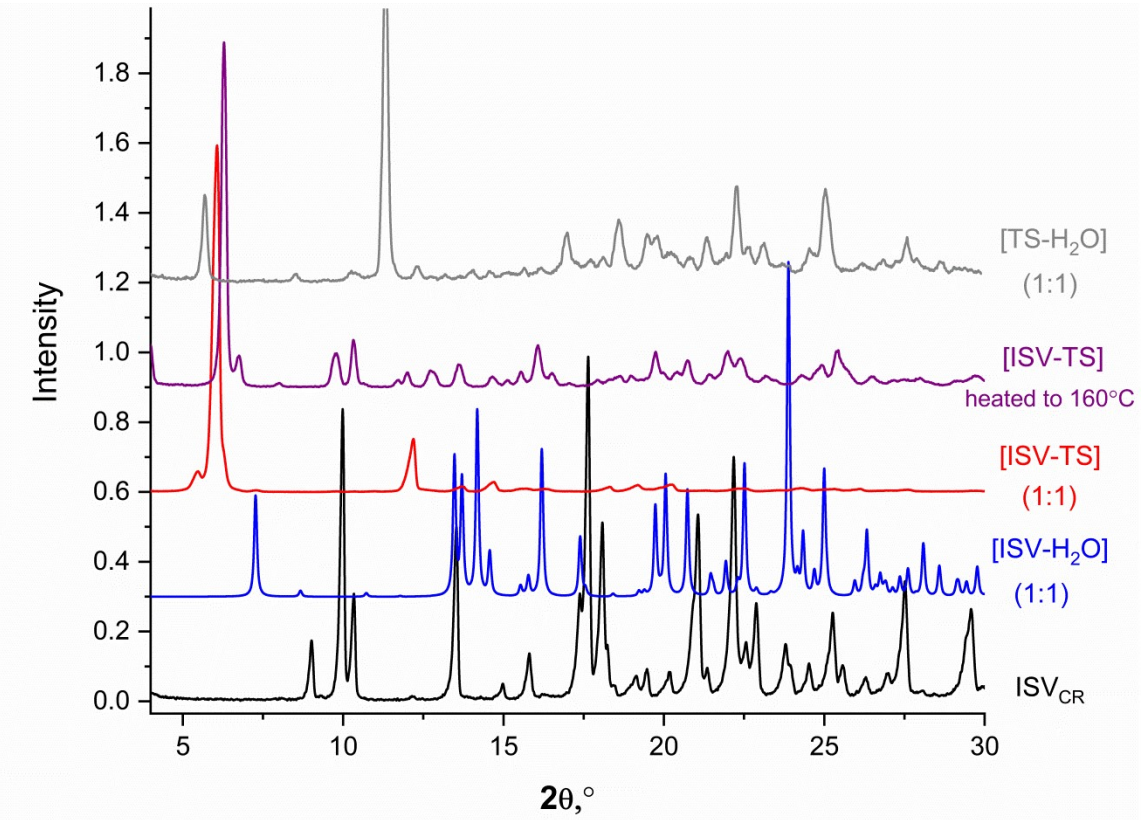

Figure S10. Powder XRD patterns of parent ISV, [ISV-H_2O] (1:1), [TS-H_2O] (1:1), unsolvated [ISV-TS] sample and high-temperature form of [ISV-TS] obtained via heating the salt up to 160°C.

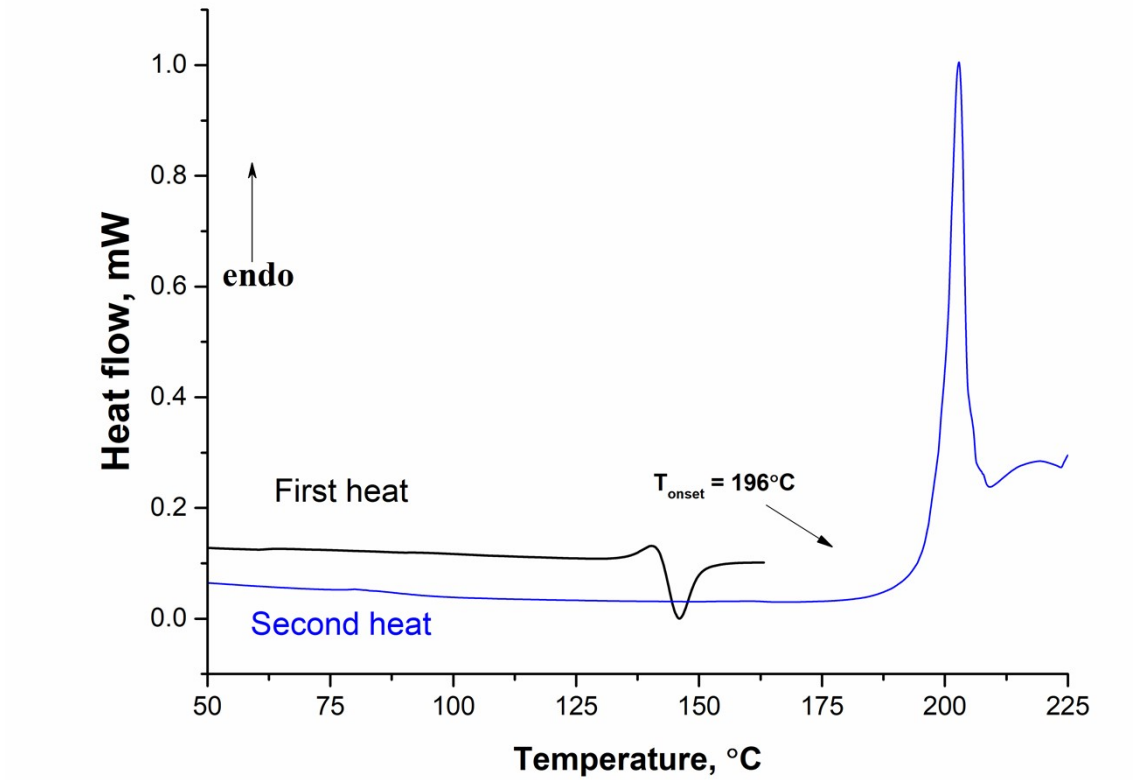

Figure S11. DSC results for the [ISV-TS] sample: initial sample (black line), after heating to 160 °C (blue line).

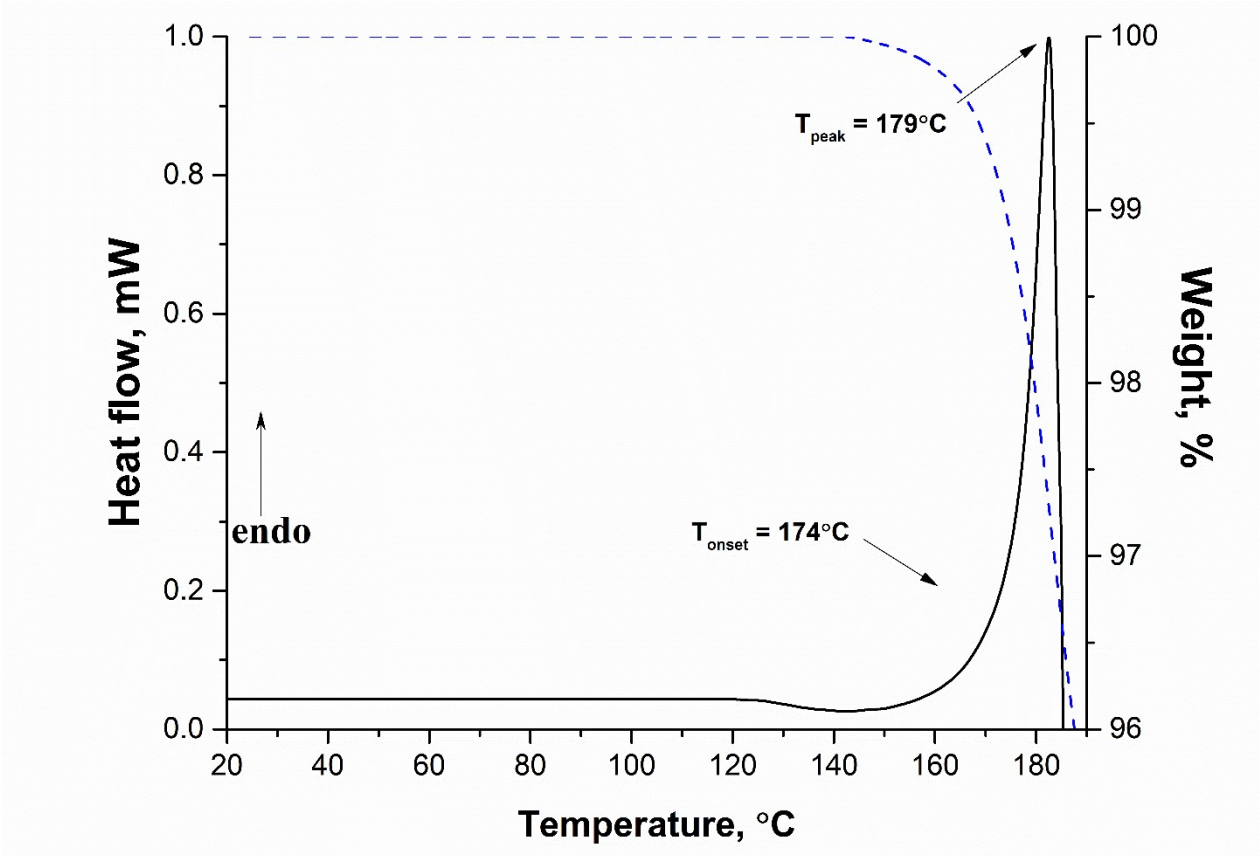

Figure S12. The results of DSC (solid line) and TG (dashed line) experiments for [ISV-P].

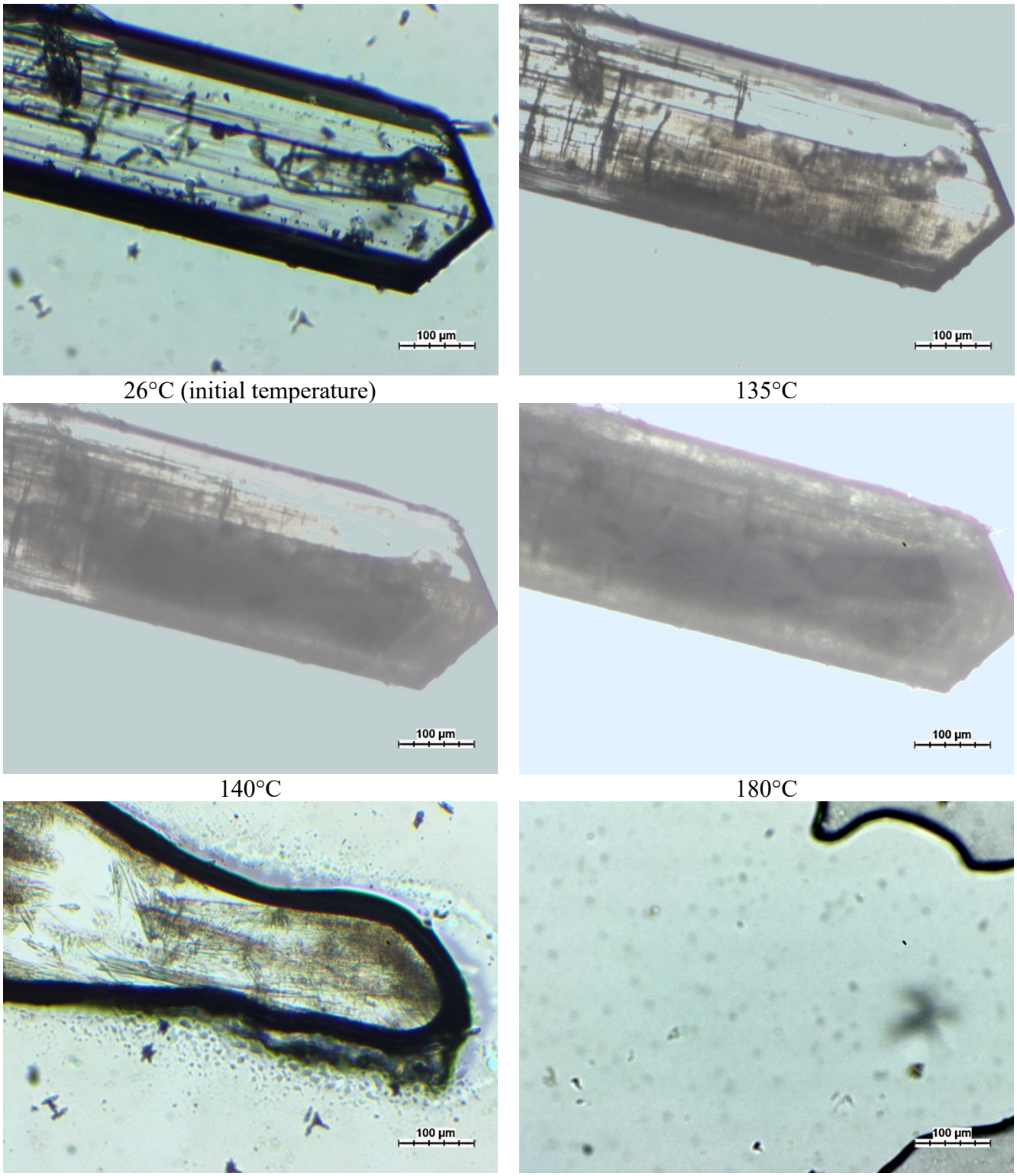

26°C (initial temperature) 135°C

140°C 180°C

196°C 200°C

Figure S13. Hot stage microscopy images of the [ISV-TS-ACN] single crystal taken at various temperatures during the sample heating.

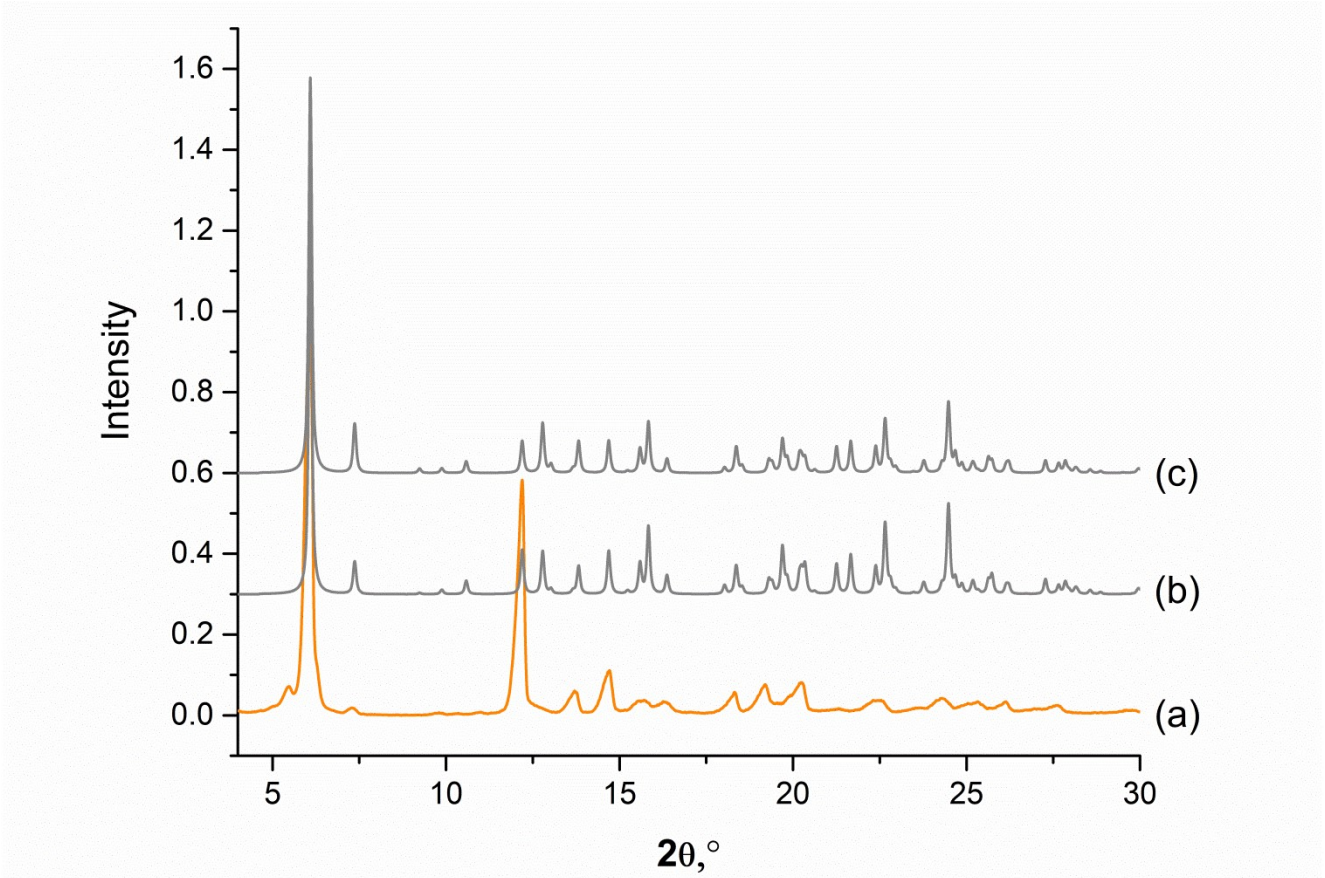

Figure S14. Overlay of experimental (a) and simulated XRD patterns of [ISV-TS] (1:1) obtained from the crystal structure (b) without and after structure relaxation (c)

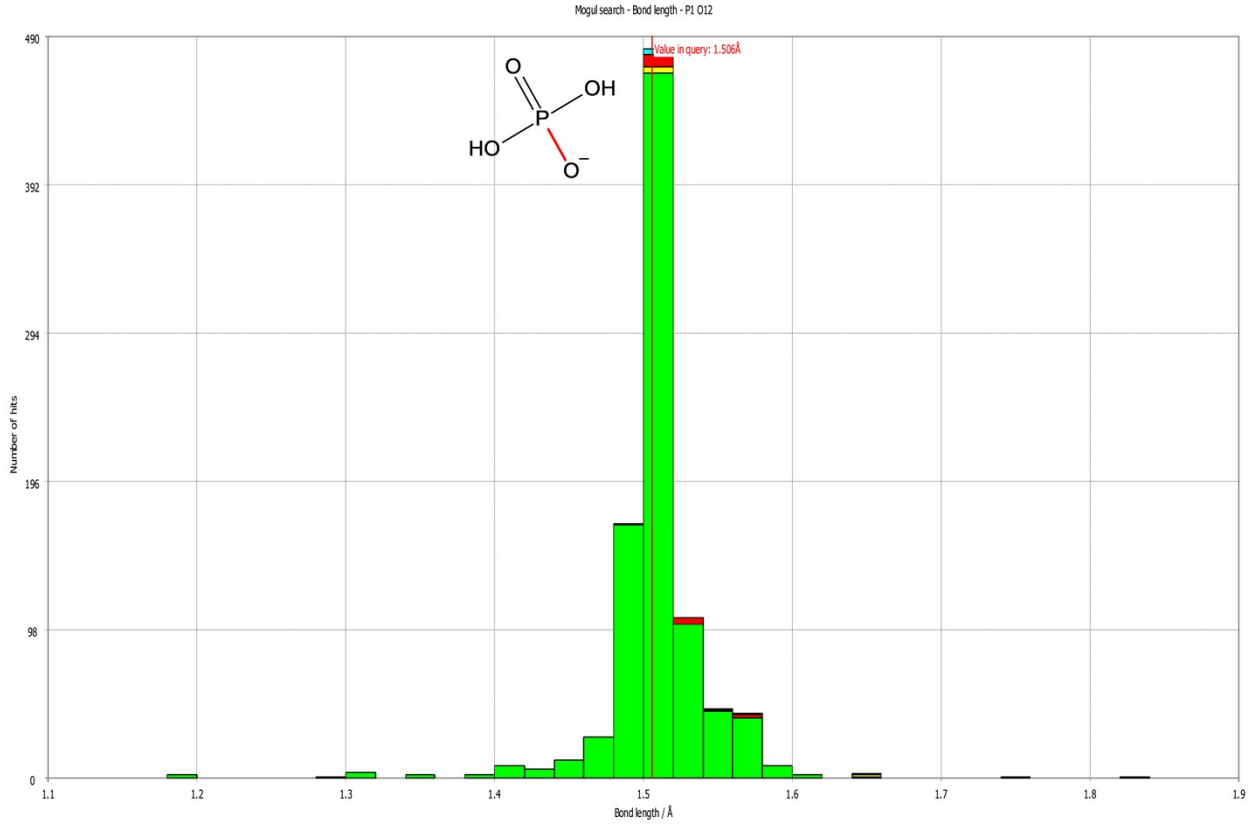

Figure S15. Results of the Mogul analysis for the P^{V}-O^{-} bond length in the CSD

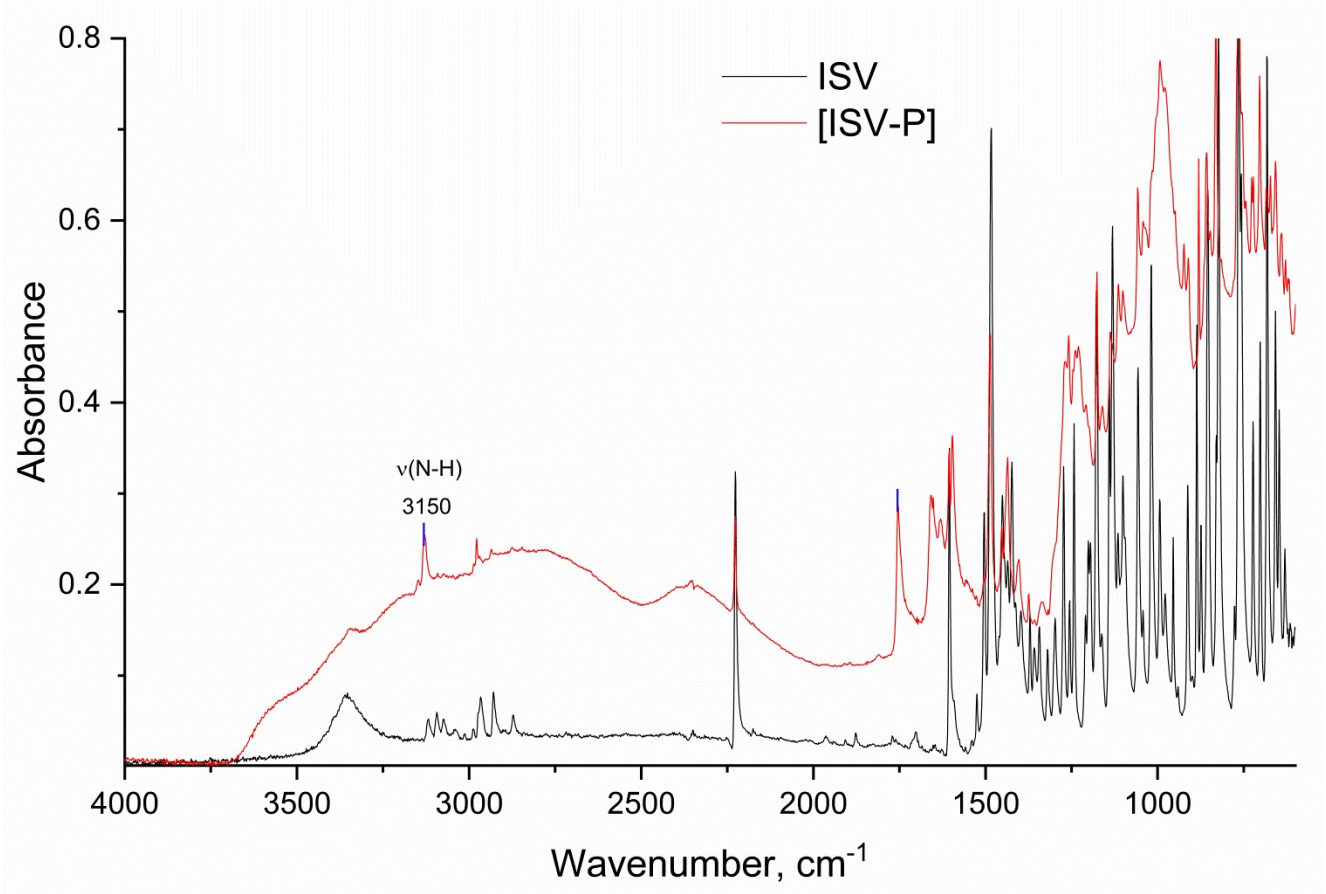

Figure S16. FTIR spectra of initial ISV_{CR} (black line) and [ISV-P] (red line). The highlighted peak corresponds to stretching of the N^{+}-H bond in the ISV cation.

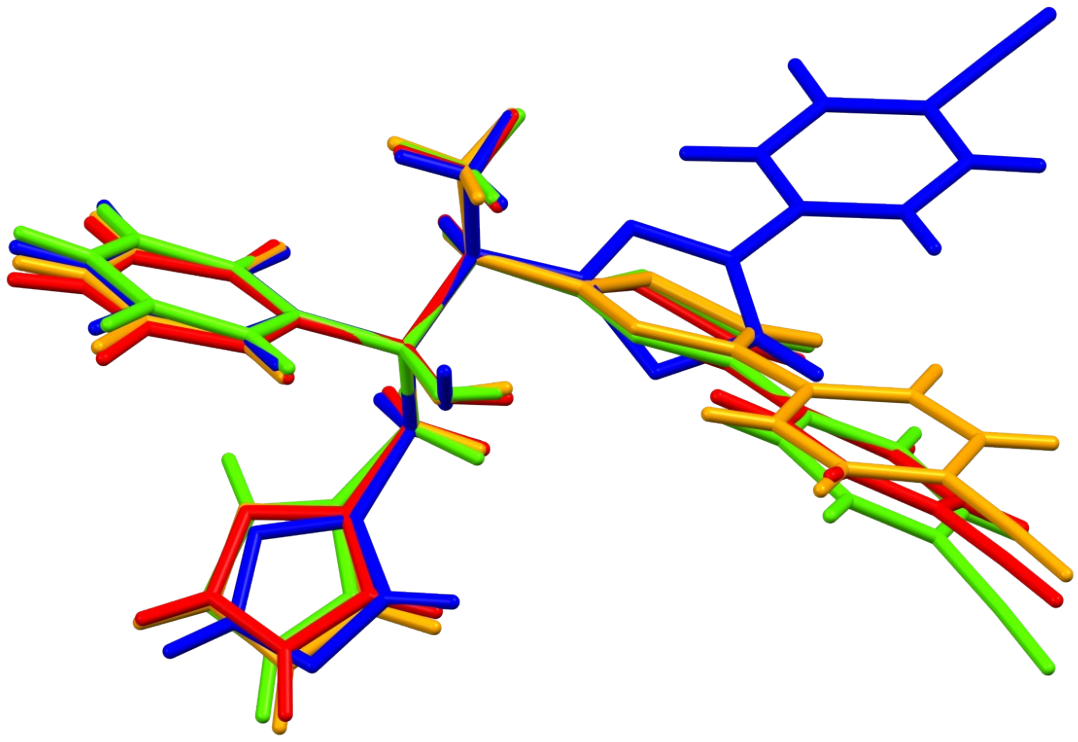

Figure S17. Overlay of the conformations of ISV molecules extracted from the crystal structures of ISV_{CR} (green), [ISV-H_2O] (blue), [ISV-TS] (red) and [ISV-P] (orange).

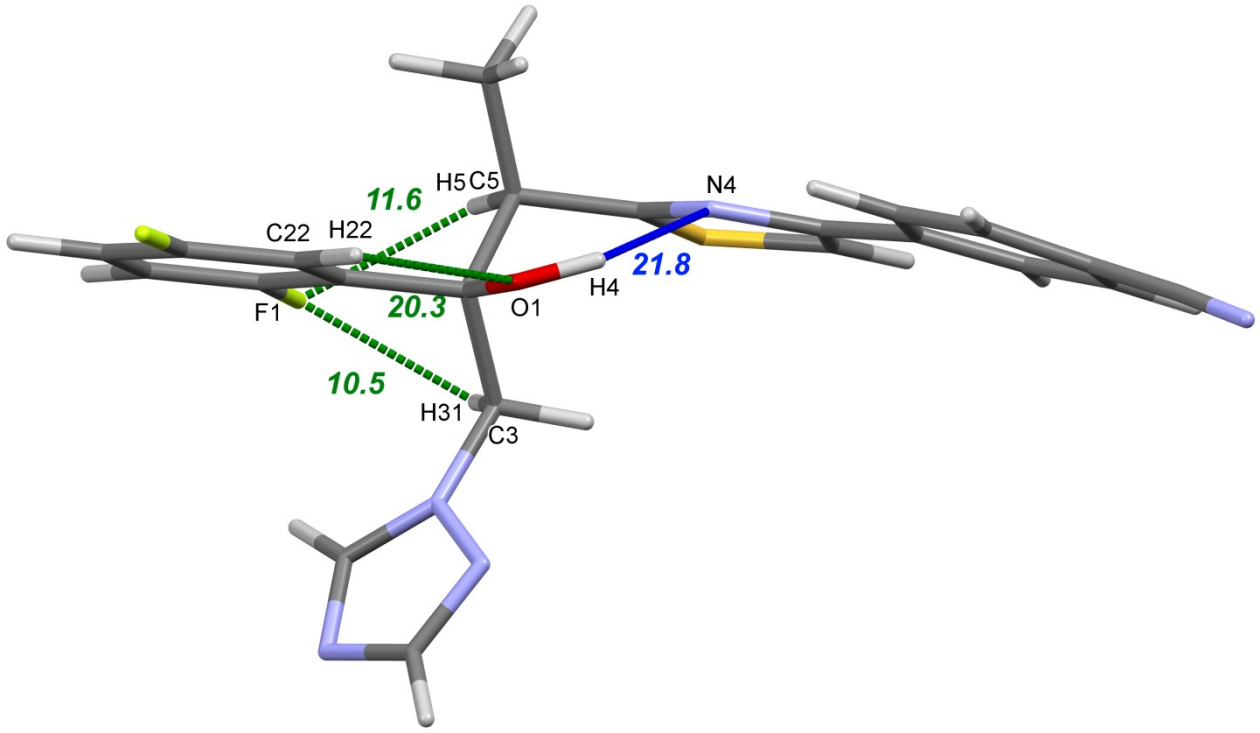

A

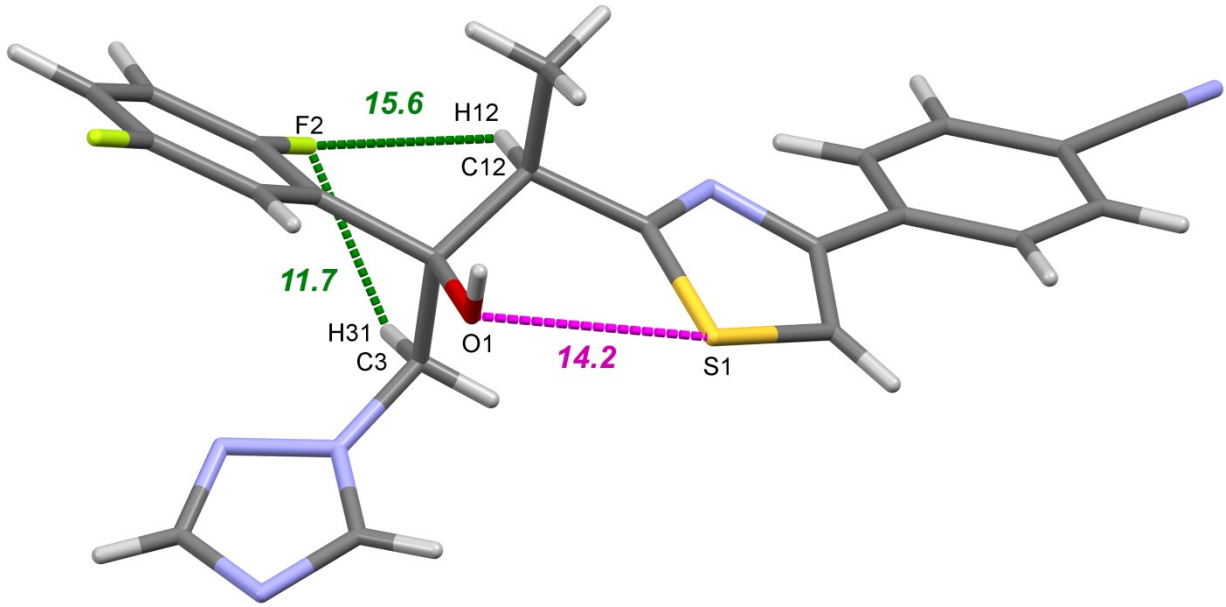

B

Figure S18. The images of "closed" (A) and "open" (B) conformations of ISV stabilized by intramolecular O-H···N bonds (blue), C-H···X hydrogen bonds (green) and chalcogen bonds (magenta). The numbers indicate energies of non-covalent interactions estimated using eq. (3). The atom numeration is consistent with that in crystals of ISV and [ISV-H_2O] (1:1).

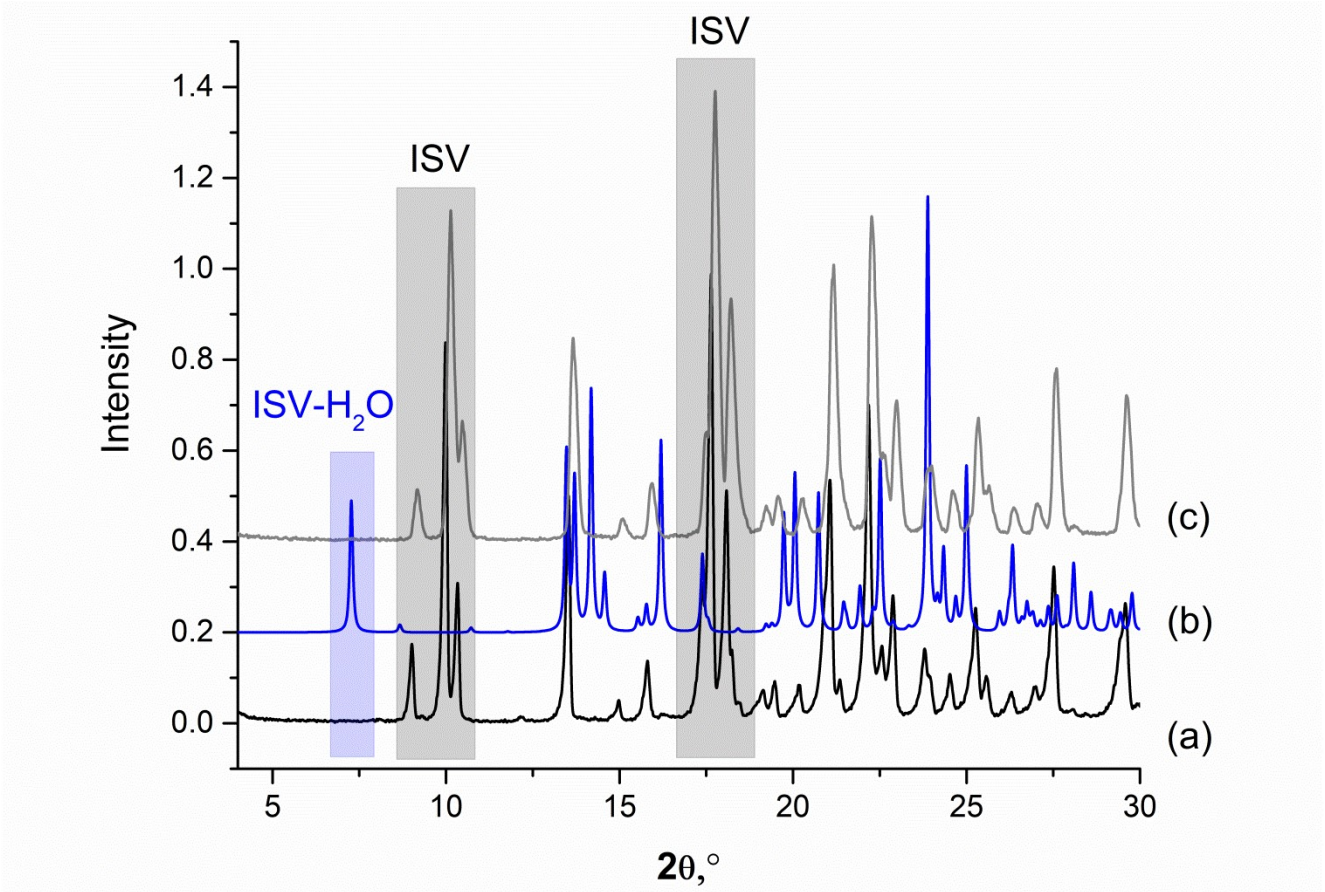

Figure S19. Experimental PXRD patterns of ISV_{CR} (a), [ISV-H_2O] (1:1) (b) and the solid phase after 48h dissolution experiments of ISV_{CR} in pH 7.4 buffer media at 37°C (c)

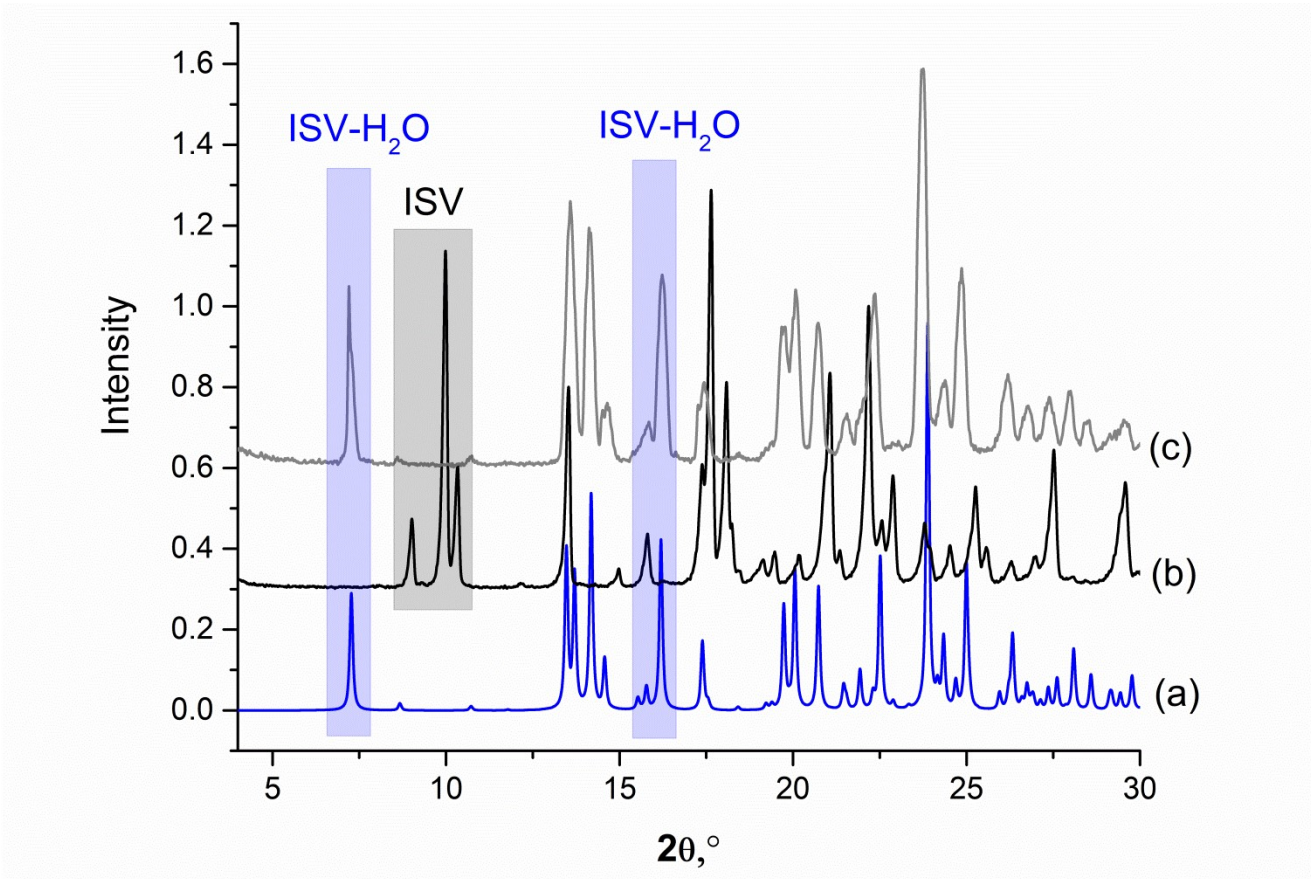

Figure S20. Experimental PXRD patterns of [ISV-H_2O] (1:1) (a), ISV_{CR} (b) and the solid phase after 48h dissolution experiments of [ISV-H_2O] (1:1) in pH 7.4 buffer media at 37°C (c)

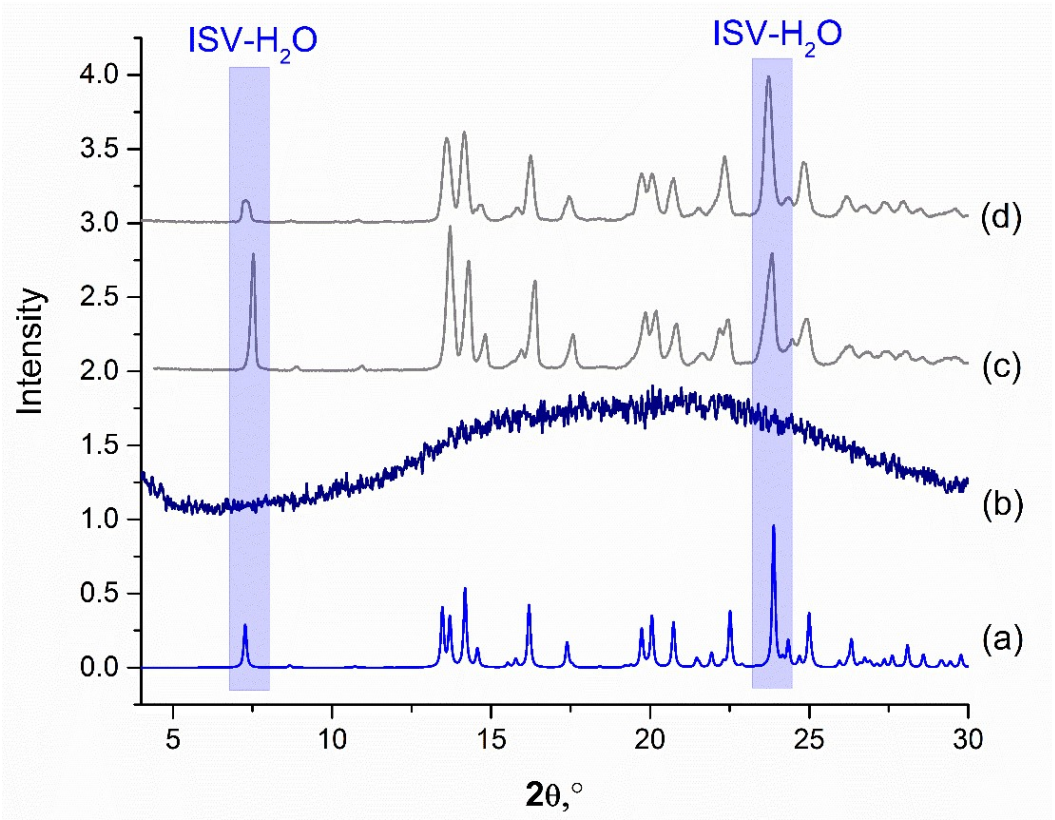

Figure S21. Experimental PXRD patterns of [ISV-H_2O] (1:1) (a), $ISV_{A,NG}$ (b) and solid phases after 24h dissolution experiments of $ISV_{A,NG}$ in pH 1.2 (c) and pH 7.4 (d) buffer media

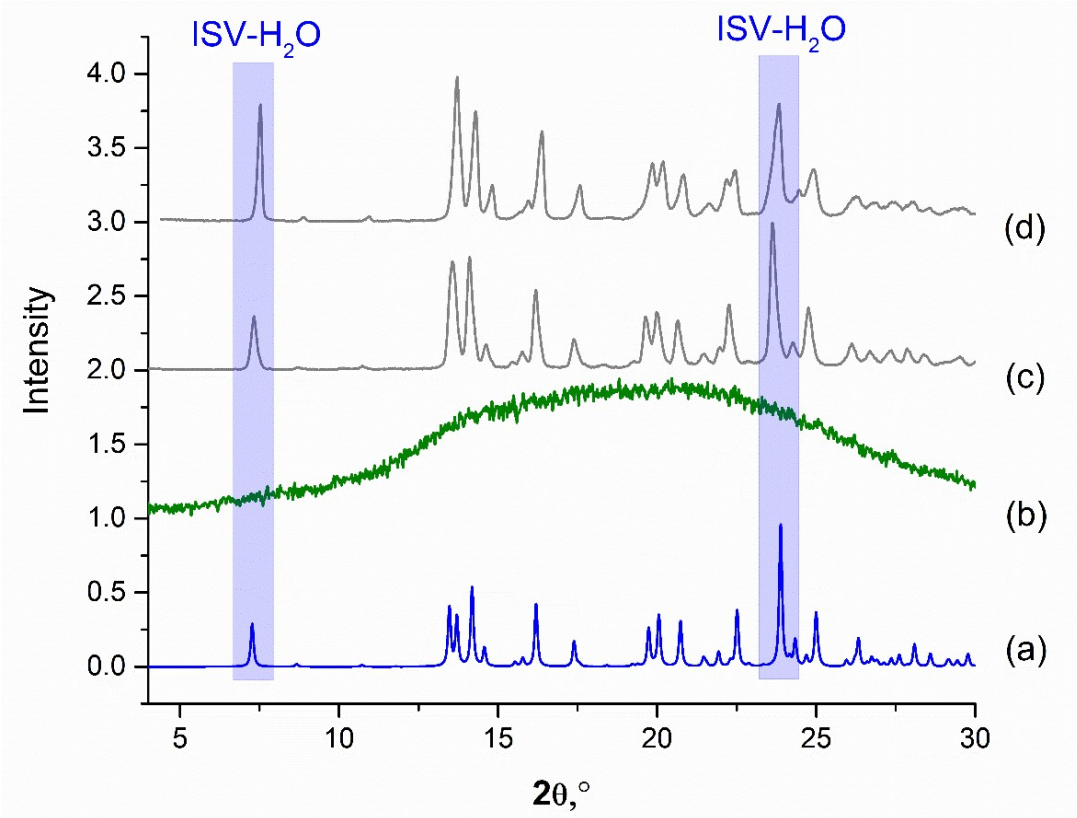

Figure S22. Experimental PXRD patterns of [ISV-H_2O] (1:1) (a), $ISV_{A,FD}$ (b) and solid phases after 24h dissolution experiments of $ISV_{A,FD}$ in pH 1.2 (c) and pH 7.4 (d) buffer media

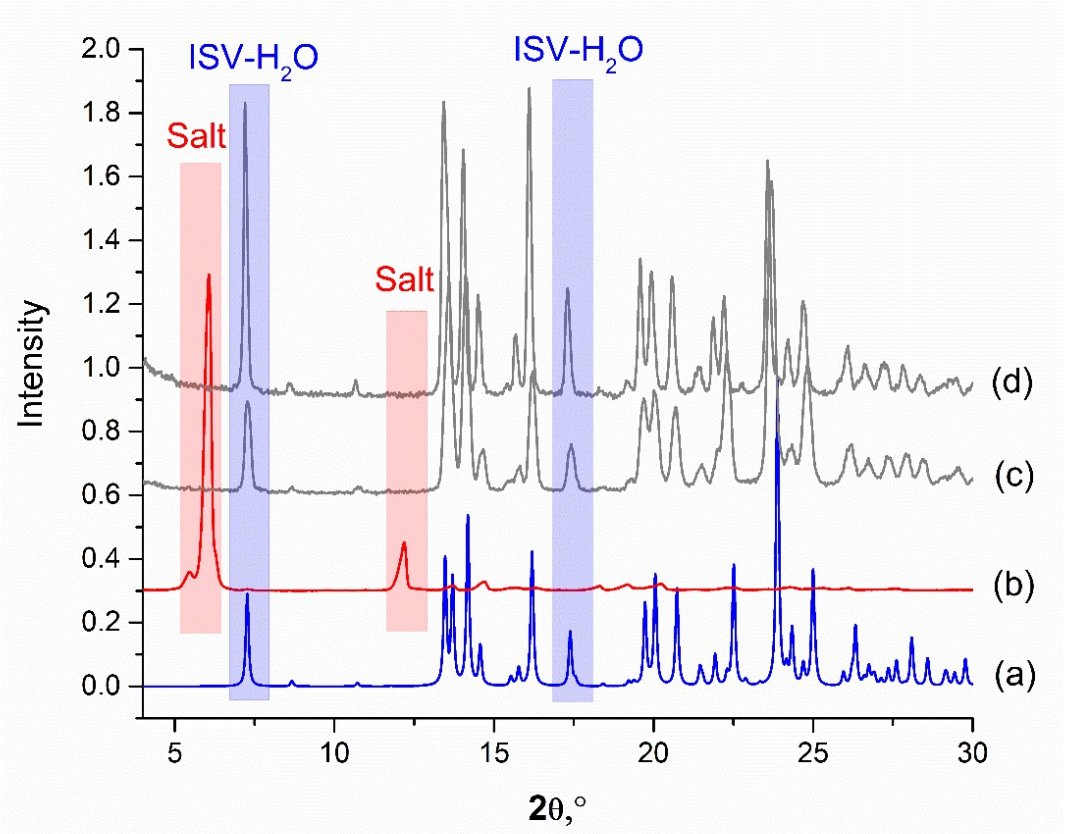

Figure S23. Experimental PXRD patterns of [ISV-H_2O] (1:1) (a), [ISV-TS] (1:1) (b) and solid phases after 24h dissolution experiments of [ISV-TS] (1:1) in pH 1.2 (c) and pH 7.4 (d) buffer media

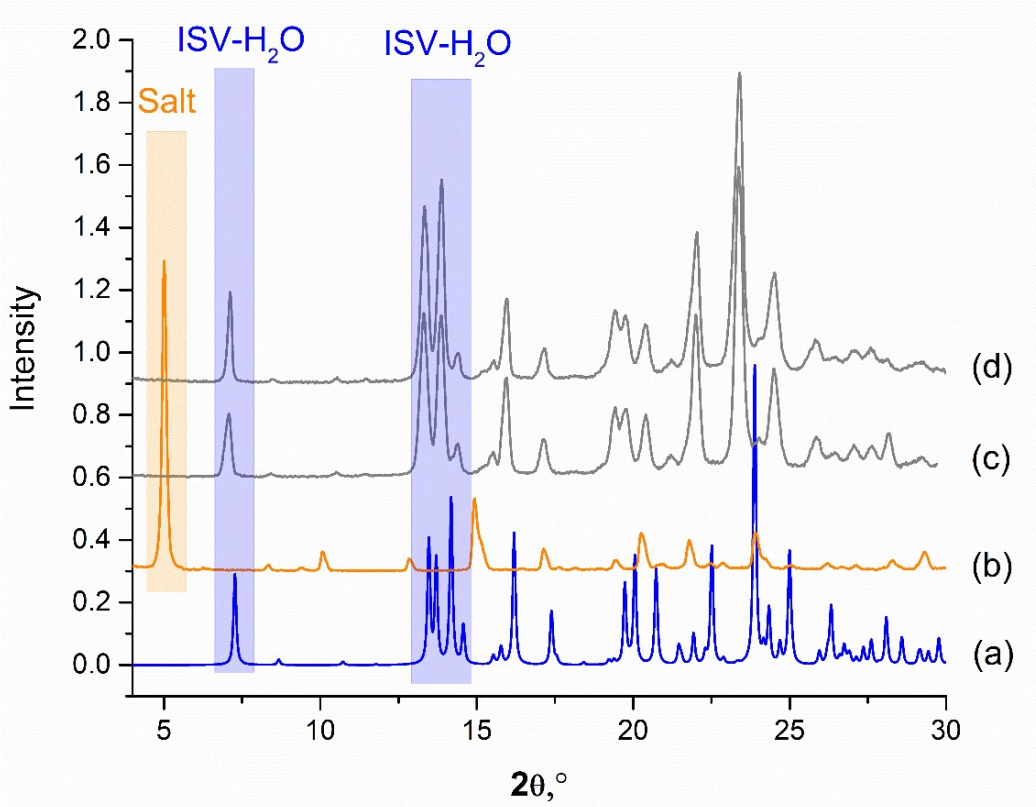

Figure S24. Experimental PXRD patterns of [ISV-H_2O] (1:1) (a), [ISV-P] (1:1) (b) and solid phases after 24h dissolution experiments of [ISV-P] (1:1) in pH 1.2 (c) and pH 7.4 (d) buffer media

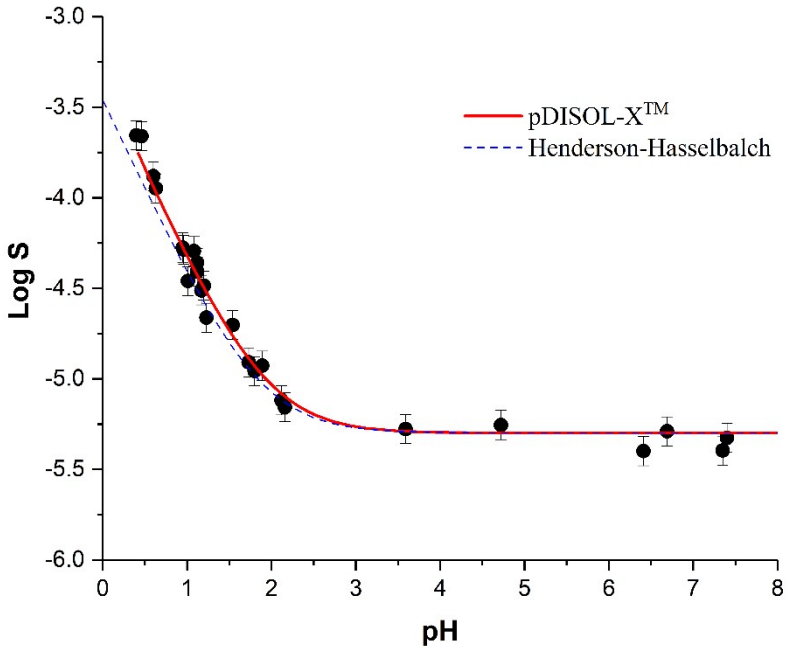

Figure S25. Experimental solubility−pH dependences for [ISV-H_2O] obtained by dissolution of [ISV-H_2O] (1:1), [ISV-P] (1:1) and [ISV-TS] (1:1) in buffer solutions with different pH values at 37 °C. The solid red line represents the best-fit refinement curve through the measured logS-pH points using the pDISOL-X™ program. The dashed blue curve refers to the profile calculated from the Henderson-Hasselbalch equation

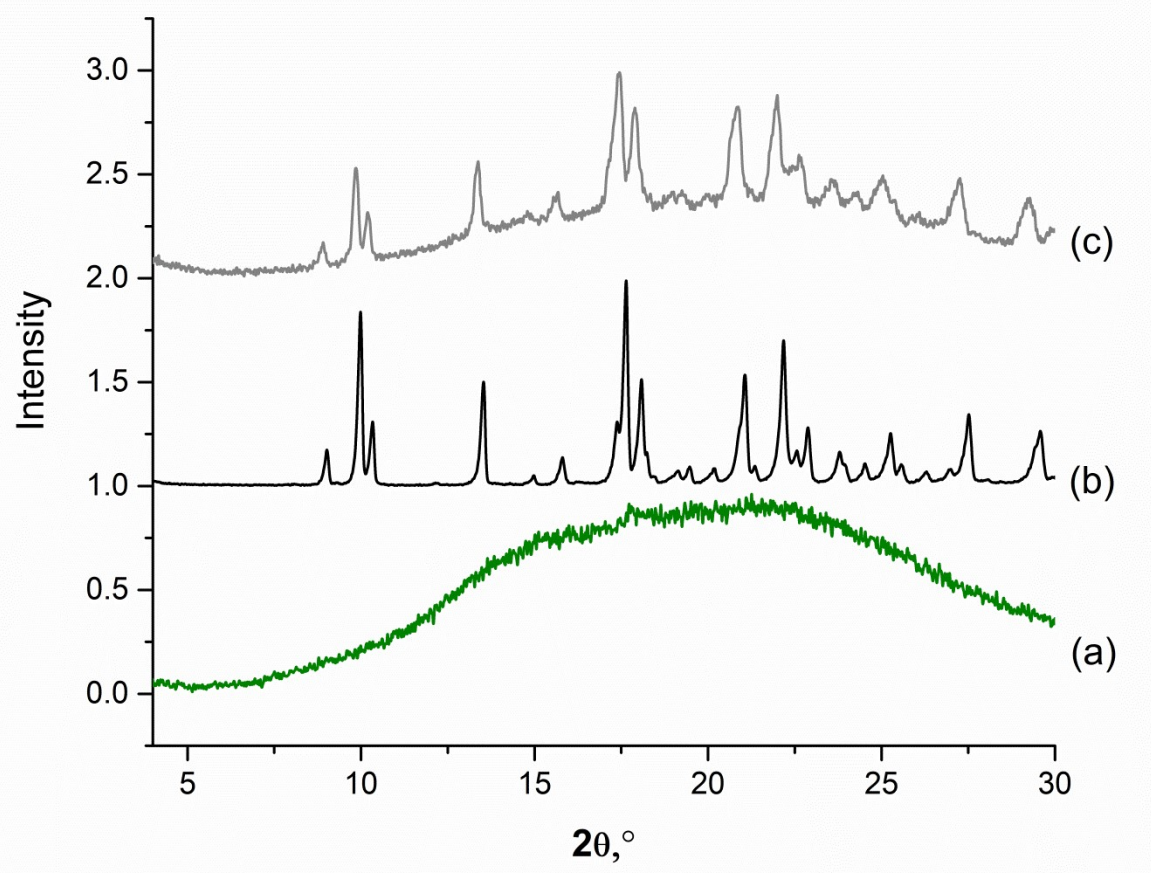

Figure S26. Experimental PXRD patterns of initial amorphous ISV (a), ISV_{CR} (b), and the surface of the pressed tablet for the dissolution tests

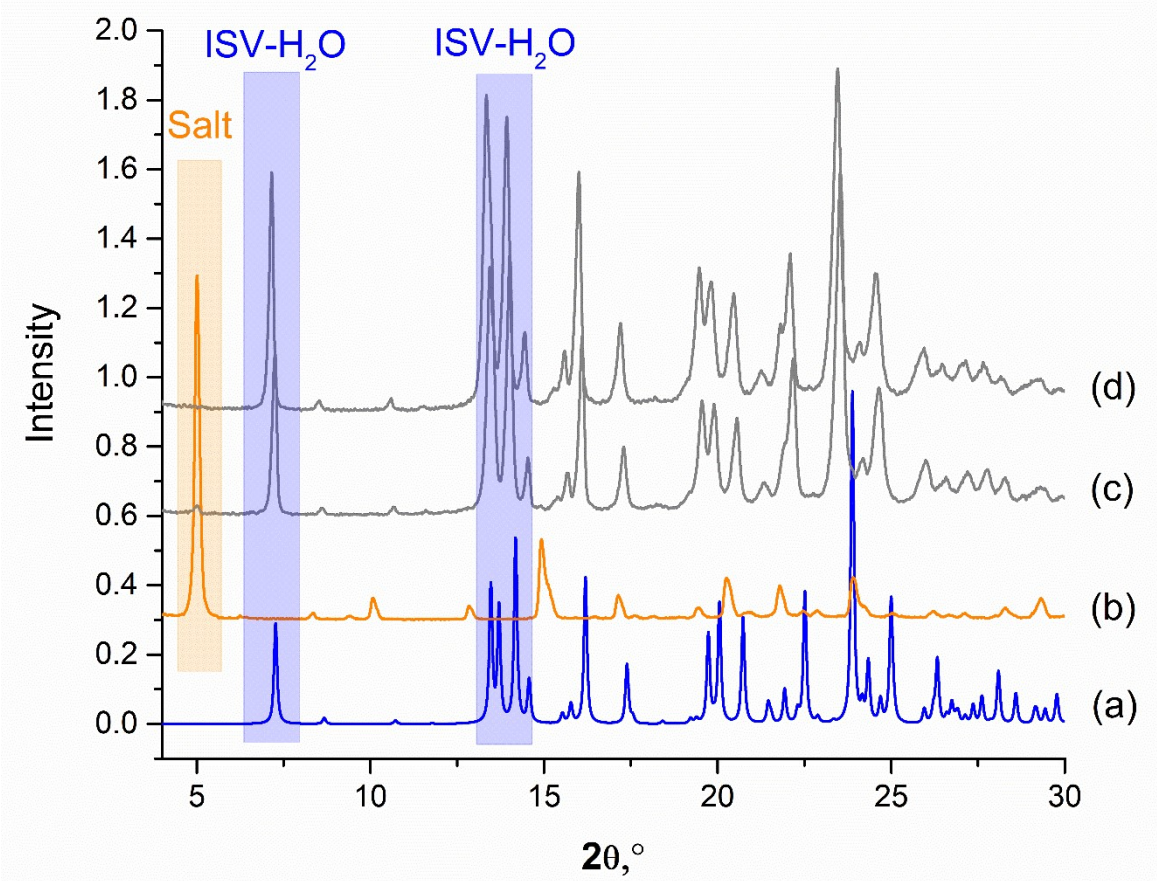

Figure S27. Experimental PXRD patterns of [ISV-H_2O] (1:1) (a), [ISV-P] (1:1) (b) and the solid phase after 8h IDR experiments of [ISV-P] (1:1) in pH 1.2 (c) and pH 7.4 (d) buffer media.

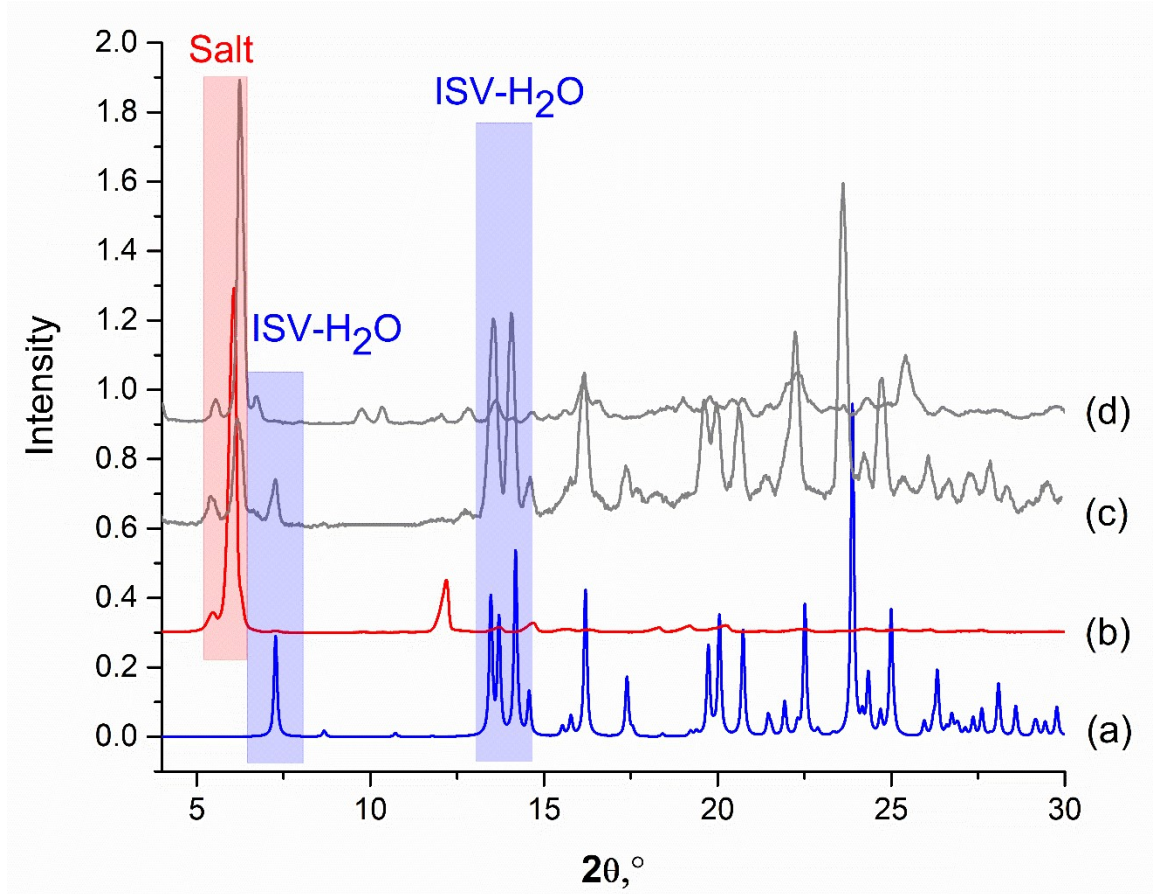

Figure S28. Experimental PXRD patterns of [ISV-H_2O] (1:1) (a), [ISV-TS] (1:1) (b), surface layer of the tablet (c) and main body of the tablet (d) after 8h IDR experiments of [ISV-TS] (1:1) in pH 1.2 buffer media.

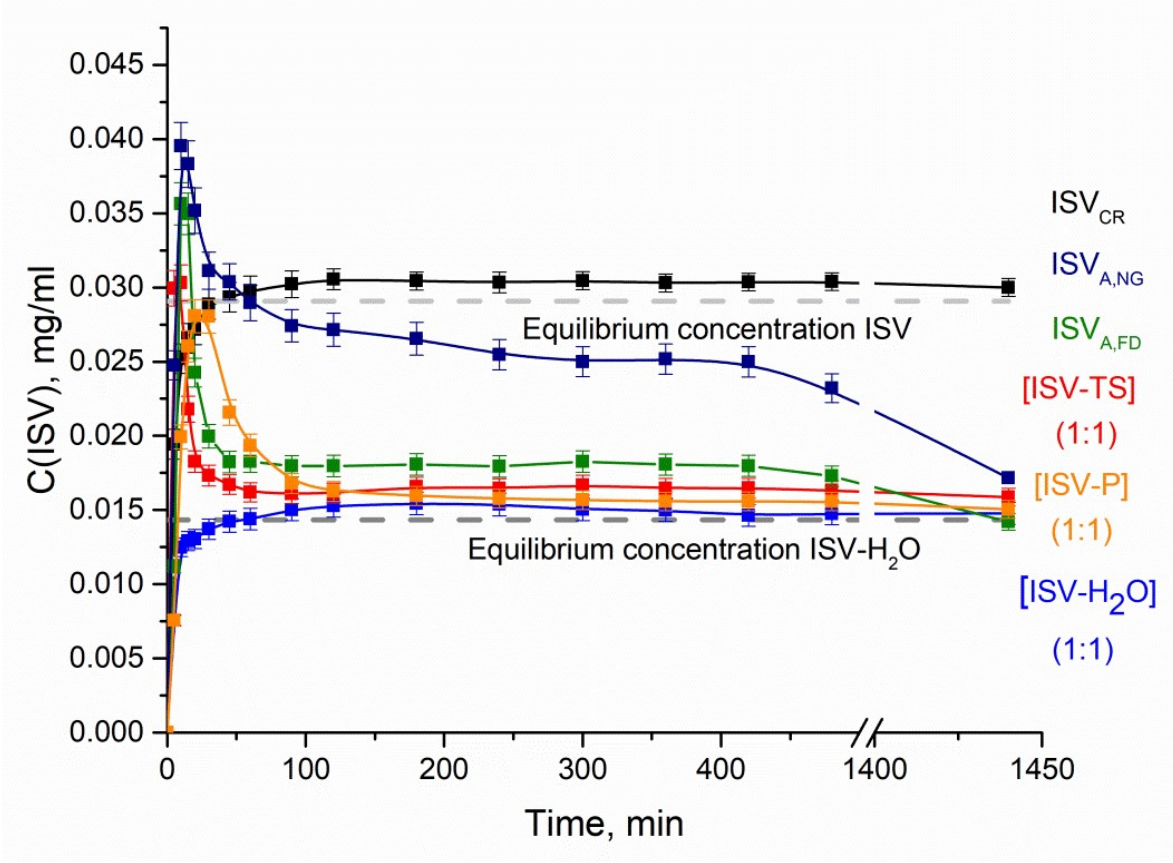

(a)

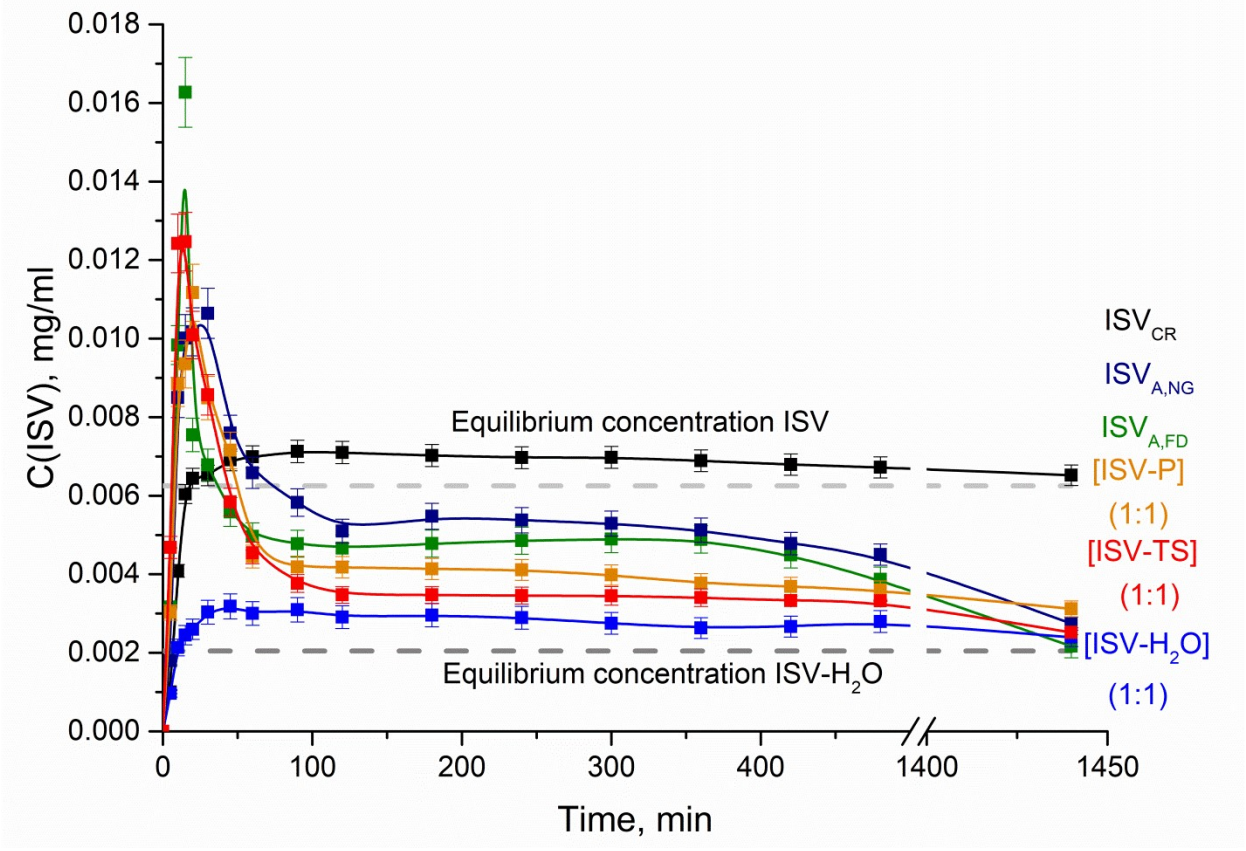

(b)

Figure S29. Dissolution curves for the initial ISV_{CR}, [ISV-H_2O] (1:1), [ISV-TS] (1:1), [ISV-P] (1:1), $ISV_{A,FD}$ and $ISV_{A,NG}$ in pH 1.2 (a) and pH 7.4 (b) buffer solutions at 37.0 ± 0.1 °C.